

RESEARCH

Open Access



Downregulation of STAT3 transcription factor reverses synaptotoxic phenotype of reactive astrocytes associated with prion diseases

Rajesh Kushwaha^{1,2}, Kara Molesworth^{1,2}, Natallia Makarava^{1,2} and Ilia V. Baskakov^{1,2*}

Abstract

In neurodegenerative diseases, including prion diseases, astrocytes adopt reactive phenotypes that persist throughout disease progression. While astrocyte reactivity may initially serve as a protective response to prion infection, it transitions into a neurotoxic phenotype that disrupts homeostatic functions and exacerbates disease pathology. The transcription factor Stat3 has been recognized as a master regulator of astrocyte reactivity in neurodegenerative diseases, yet its role in prion disease-associated astrocyte reactive phenotypes remains unexplored. The current study addresses this gap by investigating the effects of Stat3 deletion in reactive astrocytes isolated from prion-infected mice. We demonstrate that Stat3 deletion mitigates the reactive astrocyte phenotype and alleviates their synaptotoxic effects. Stat3-dependent activation of astrocytes was reproduced by co-culturing naïve astrocytes with reactive microglia isolated from prion-infected animals or exposing them to microglia-conditioned media. A cytokine array profiling of 40 molecules revealed partially overlapping inflammatory signatures in reactive microglia and astrocytes, with IL-6 prominently upregulated in both cell types. Notably, IL-6 treatment elevated phosphorylated Stat3 levels in naïve astrocytes and triggered astrocyte reactivity. These findings indicate that the synaptotoxic phenotype of astrocytes in prion diseases can be sustained by reactive microglia and self-reinforced in a cell-autonomous manner. Our work highlights the pivotal role of Stat3 signaling in astrocyte activation and suggests that Stat3 inhibition may suppress the reactive phenotype of astrocytes associated with prion diseases.

Keywords Prions, Prion diseases, Reactive astrocytes, Reactive microglia, Stat3 transcription factor, Neuroinflammation, Interleukin 6

*Correspondence:

Ilia V. Baskakov

Baskakov@som.umaryland.edu

¹Center for Biomedical Engineering and Technology, University of Maryland School of Medicine, 111 S. Penn St, Baltimore, MD 21201, USA

²Department of Neurobiology, University of Maryland School of Medicine, Baltimore, MD 21201, USA



© The Author(s) 2025. **Open Access** This article is licensed under a Creative Commons Attribution-NonCommercial-NoDerivatives 4.0 International License, which permits any non-commercial use, sharing, distribution and reproduction in any medium or format, as long as you give appropriate credit to the original author(s) and the source, provide a link to the Creative Commons licence, and indicate if you modified the licensed material. You do not have permission under this licence to share adapted material derived from this article or parts of it. The images or other third party material in this article are included in the article's Creative Commons licence, unless indicated otherwise in a credit line to the material. If material is not included in the article's Creative Commons licence and your intended use is not permitted by statutory regulation or exceeds the permitted use, you will need to obtain permission directly from the copyright holder. To view a copy of this licence, visit <http://creativecommons.org/licenses/by-nc-nd/4.0/>.

Introduction

Astrocytes and microglia transitioning into reactive states are well-recognized hallmarks of neurodegenerative diseases such as Alzheimer's (AD), Parkinson's, and prion diseases [1, 2]. In recent years, there has been growing acknowledgment that reactive astrocytes play a complex and critical role in chronic neurodegeneration [3–6]. Nevertheless, their precise contribution to the pathogenesis of the neurodegenerative diseases and other neurological conditions remains a topic of active investigation and debate (reviewed in [4, 7–9]).

Prion diseases, also known as Transmissible Spongiform Encephalopathies, constitute a group of invariably fatal neurodegenerative disorders affecting both humans and animals [10]. These diseases are uniformly lethal and currently have no effective therapeutic options [11]. Prion diseases are initiated by prions, or PrP^{Sc}, which are misfolded, aggregated forms of the cellular prion protein or PrP^C, a sialoglycoprotein expressed in host tissues [12–16]. The pathogenesis involves prion replication and dissemination throughout the central nervous system (CNS), driven by the recruitment and conversion of host-expressed PrP^C into the misfolded PrP^{Sc} conformation [17].

In prion diseases, astrocytes adopt reactive phenotypes that persist throughout disease progression [18, 19]. Transcriptomic analyses reveal that astrocytes respond to prion infection earlier and more robustly than neurons [20–23]. Prion-infected mice exhibit widespread dysregulation of genes critical for astrocyte-specific homeostatic functions, including those involved in blood brain barrier (BBB) integrity, transporter activity, myelination, energy metabolism, ion channel regulation, extracellular matrix organization, growth factor production, receptor signaling, and neuroprotection [19, 23]. Notably, genes essential for neuronal support, as well as synapse formation and maintenance, are markedly downregulated [19, 23].

Gene expression profiling across animal groups challenged with various prion strains demonstrated a strong inverse correlation between the extent of astrocyte reactivity and the incubation period to prion disease. This suggests that reactive astrocytes play a contributory role in disease progression [19]. Supporting this hypothesis, reactive astrocytes isolated from prion-infected animals were shown to exert harmful effects on primary neuronal cultures, reducing spine size and density and impairing neuronal growth and synaptic integrity [24]. Likewise, reactive astrocytes derived from prion-infected mice induced a disease-associated phenotype in endothelial cells from non-infected adult mice [25]. Furthermore, selective inhibition of PERK signaling, a key component of the unfolded protein response that is heightened in reactive astrocytes during prion infection, extended the

incubation period to terminal disease [26]. In summary, while astrocyte reactivity may initially represent a physiological response to prion infection, it transitions into a disease-associated state that disrupts homeostatic functions and exacerbates disease pathology.

Cellular signaling mediated by Janus Kinase 2 (JAK2) and Signal Transducer and Activator of Transcription 3 (Stat3) represents a key signal transduction pathway. Activation of the Stat3 transcription factor is widely recognized as a hallmark of astrocyte reactivity in neurodegenerative diseases, consistently documented across multiple species and brain regions [4]. Targeted inhibition of the Stat3 pathway in astrocytes has been demonstrated to attenuate their activation or revert their reactive phenotype, resulting in improved outcomes in animal models of Alzheimer's disease [27–29]. While Stat3 activation has also been observed in prion-infected animals [30], its precise role in shaping the astrocyte reactive phenotype in the context of prion diseases has never been explored.

To elucidate the role of Stat3 in astrocyte reactivity associated with prion diseases, we employed the Aldh1l1-CreERT-Stat3-floxP mouse model. In this system, Cre recombinase fused to the estrogen receptor is expressed under the astrocyte-specific Aldh1l1 promoter, enabling the conditional knockout of Stat3 in astrocytes. Our findings demonstrate that the Stat3 signaling pathway is pivotal for astrocyte activation in prion diseases and that the reactive phenotype of astrocytes can be markedly suppressed by Stat3 deletion.

Materials and methods

Reagents and kits

Sodium bicarbonate, Poly-L-lysine (PLL), Poly-D-lysine (PDL), paraformaldehyde (PFA), bovine serum albumin (BSA), normal goat serum (NGS), tween 20, triton-X-100, CellLytic MT mammalian cell lysis buffer, protease inhibitor cocktail, laminin, ponceau S, dimethyl sulfoxide, methanol, hydrochloric acid and 4-hydroxytamoxifen (Sigma, St. Louis, MO); Trypsin-EDTA, Dulbecco's modified eagle medium: F12 (DMEM/F12), neurobasal medium, B27 supplement, N2 supplement, G5 supplement, trypsin inhibitor, Hank's balanced salt solution (HBSS), phosphate buffer saline (PBS), Dulbecco's phosphate buffered saline (DPBS), glutamax, L-glutamine heparin, antibiotic-antimycotic, penicillin/streptomycin and protein ladder (Invitrogen, Carlsbad, CA); VECTASHIELD mounting medium with DAPI (Vector Laboratories Burlingame, CA); supersignal west pico PLUS Chemiluminescent Substrate (Thermo Scientific, Rockford, IL), aurum Total RNA Mini Kit, SYBR Green and iScript cDNA Synthesis Kit (Bio-Rad Laboratories, Hercules, CA, CA). Recombinant mouse IL-6, proteome profiler array- mouse cytokine array panel A (R&D Systems,

Minneapolis, MN); Bicinchoninic acid (BCA) protein assay kit, 70 μm nylon mesh filter, 0.22 μm filter, MTT (3-(4,5-dimethylthiazol-2-yl)-2,5-diphenyltetrazolium bromide), polyvinylidene fluoride (PVDF) membrane (Millipore, Temecula, CA); protease/phosphatase inhibitor (Cell Signaling Technology, Danvers, MA).

Antibodies

Rabbit monoclonal antibody to Stat3 (#8768), phospho-Stat3 (#9145) and GFAP (#12389) were from Cell Signaling Technology (Danvers, MA). Rabbit monoclonal antibodies to synaptophysin (#ab32594), Drebrin (#ab11068), olig2 (#ab136253) and chicken monoclonal antibody to MAP2 (#ab4542) were from Abcam (Cambridge, MA). Chicken polyclonal antibody to GFAP (#AB5541), mouse monoclonal antibodies to β -actin (#A5441), horseradish peroxidase (HRP) conjugated secondary anti-rabbit IgG (cat. A0545) and anti-mouse IgG (#A9044) were from Sigma-Aldrich (St. Louis, MO). Anti-ACSA-2 MicroBead Kit (#130-097-678) and CD11b MicroBeads (#130-049-601) was from Miltenyi Biotec (Bergisch Gladbach, Germany). Alexa Fluor 488 goat anti-rabbit IgG, Alexa Fluor 488 goat anti-chicken IgG, Alexa Fluor 488 goat anti-mouse IgG, Alexa Fluor 546 goat anti-rabbit IgG and Alexa Fluor 546 goat anti-mouse IgG secondary antibodies were purchased from Invitrogen (Carlsbad, CA). Rabbit polyclonal antibody to complement C3 (#PA5-21349, ThermoFisher Scientific, Waltham, MA); mouse monoclonal antibody to PSD-95 (#75028020, Antibodies Incorporated, (Davis, CA); rabbit polyclonal antibody to Iba1 (#01919741, Wako, Richmond, VA).

Animals

For conditional knockout of Stat3 in astrocytes, Aldh1l1-CreERT-Stat3-floxP mouse model was used [31]. Heterozygous (Aldh1l1-CreERT)^{+/-}(Stat3-floxP)^{+/+} females and homozygous (Stat3-floxP)^{+/+} males that are CreERT-negative were used to produce (Aldh1l1-CreERT)^{+/-}(Stat3-floxP)^{+/+} and (Stat3-floxP)^{+/+} littermates. Seven to eight week-old Cre^{+/-} and Cre^{-/-} male and female mice were intraperitoneally inoculated with 200 μl volume of 1% 22 L mouse-adapted prion strain in PBS under anesthesia. Animals were scored for disease progression as previously described [32]. Mice were considered terminally ill upon a loss of 20% body weight. Mice were euthanized at the terminal stage, and their brains dissected out in dissection buffer.

Isolation and culturing of primary astrocytes

Astrocyte isolation and culturing were performed as previously described [33] using magnetic-activated cell sorting (MACS, Miltenyi Biotec). Briefly, cortical brain tissues were dissociated into single-cell suspensions using

an Adult Brain Dissociation Kit (#130-107-677, Miltenyi Biotec) according to the manufacturer's instructions. The brain were quickly harvested, and cortical tissue was dissected out (one brain per isolation) and kept in cold DPBS. Meninges were carefully removed. Cortical tissue was cut into small pieces and then transferred into gentleMACS C tubes (#130-093-237, Miltenyi Biotec) that contained 1950 μL of enzyme mixture 1 solution and 30 μL of enzyme mixture 2 solution. Tissue dissociation was performed in the C-tubes using the program 37C_ABDC_01 (30 min) of the gentleMACS Octo Dissociator with Heaters (#130-096-427, Miltenyi Biotec), allowing for simultaneous enzymatic and mechanical disruption. The obtained dissociated cells were re-suspended in cold DPBS, filtered through 70 μm MACS SmartStrainer to remove non-dissociated tissue, and then centrifuged at 1000 rpm for 10 min. The cell pellets were re-suspended in cold DPBS, and the cell suspension was subjected to debris and red blood cell removal. Then, the single-cell suspension was subjected to magnetic labeling using the Anti-ACSA-2 (astrocytes cell surface antigen-2) MicroBead Kit (#130-097-678, Miltenyi Biotec) according to the manufacturer's instructions. The cell suspension was blocked with 10 μL of FcR blocking reagent at 4°C for 10 min, then labeled with 15 μL of Anti-ACSA-2 MicroBeads per 10⁷ total cells via incubating for 15 min at 4°C in the dark. After labelling, the cells were washed with 2 mL of AstroMACS separation buffer (#130-117-336, Miltenyi Biotec) and centrifuged at 1500 rpm for 5 min to remove excess beads. The obtained cell pellets were re-suspended in buffer and loaded onto an LS Column (#130-042-401, Miltenyi Biotec) that was placed in the magnetic field of a MACS magnetic cell separator (#130-108-933). The column was washed with the 3mL of buffer, allowing unlabelled, ACSA-2 negative cells to wash off the column. After the wash, the column was removed from the magnetic separator, and the astrocyte-enriched population was eluted using the same buffer. The ACSA-2-positive cell fraction was collected, centrifuged and re-suspended in complete AstroMACS Medium (#130-117-031, Miltenyi Biotec) supplemented with 50 U/ml penicillin/streptomycin, 0.25% L-glutamine (0.5 mM) and serum-free AstroMACS supplements. Cells were then seeded onto poly-L-lysine (PLL) and laminin-coated chamber slides or culture flasks at a plating density of 3-4 $\times 10^4$ per chamber slide or 7 $\times 10^5$ per flask and grown in a humidified CO₂ incubator at 37°C with 5% CO₂. The media was changed after one day of culturing to remove debris and unattached dead cells. Primary astrocytes were cultured in a serum-free medium for two to three weeks until 80% confluency. The purity of astrocyte cultures was confirmed by co-immunostaining of GFAP with Iba1, Olig2 and NeuN.

For experiments that use naive astrocytes, astrocytes were isolated from non-infected, 140–180-day old Cre^{+/-} mice. In the experiment on IL-6 treatment, astrocytes isolated from adult Cre^{+/-} mice were cultured with 100 ng/ml recombinant mouse IL-6 for 72 h and analyzed.

Isolation and culturing of primary microglia

Primary microglia isolation and culturing were performed as previously described [34] using MACS method (Miltenyi Biotec) with some modifications. Brain tissues were enzymatically dissociated using the Adult Brain Dissociation Kit (#130-107-677, Miltenyi Biotec) according to the manufacturer's instructions. Briefly, the cortical brain tissues were dissected, transferred into gentleMACS C tubes (#130-093-237, Miltenyi Biotec) containing an enzyme mixture and incubated on a rotating gentleMACS Octo Dissociator (Miltenyi Biotec) for 30 min. The resulting cell suspension was then re-suspended in cold DPBS, filtered through 70 µm MACS SmartStrainer for removing undissociated tissue, and centrifuged at 1000 rpm for 10 min. The obtained cell pellets were re-suspended in cold DPBS, the myelin and cell debris were removed using a debris removal solution, then erythrocytes were removed using a red blood cell removal solution. The single cell suspension obtained was subjected to magnetic labeling with an Anti-CD11b MicroBead (#130-049-601, Miltenyi Biotec) according to the manufacturer's instructions. 15 µL of Anti-CD11b MicroBeads was added to the cell suspension, mixed well and incubated for 15 min at 4°C in the dark. The cells were washed by adding 2 mL of a buffer (PBS + 0.5%BSA) and centrifuged at 1500 rpm for 5 min. The cell pellets were re-suspended in the buffer and loaded onto an LS Column, which was placed in the magnetic field of a MACS magnetic cell separator. After washing the column with the buffer, the column was removed from the magnetic separator, and the purified microglia (CD11b-positive) fraction was eluted by flushing the column with the buffer. The CD11b positive cell fraction was centrifuged and re-suspended in complete growth media (DMEM/F12 containing 365 µg/mL l-glutamine, 1 mM sodium pyruvate; 1% heat-inactivated FBS; 100 U/mL penicillin and 100 µg/mL streptomycin). Then, cells were seeded onto PLL-coated chamber slides or culture flasks at a plating density of 3–4 × 10⁴ per chamber slide or 7 × 10⁵ per flask and grown in a humidified CO₂ incubator at 37°C with 5% CO₂.

Preparation of 4-hydroxytamoxifen and cell treatment

4-hydroxytamoxifen (#H7904, Sigma-Aldrich) was first dissolved in cell culture grade ethanol and then diluted in PBS. In all experiments including the experiments on neuron-astrocyte or microglia-astrocytes co-cultures, primary astrocyte were treated with 1 µM

4-hydroxytamoxifen (TAM) or PBS containing 0.02% ethanol (mock treatment) for 72 h.

Astrocytes-microglia co-cultures

Astrocytes and microglia were co-cultured as previously described [35, 36] with slight modifications. Briefly, ACSA-2-positive astrocytes were cultured in a humidified CO₂ incubator at 37°C with 5% CO₂ for one week at a density of 3–4 × 10⁴ per chamber slide or 3.5–4 × 10⁵ per well plate. CD11b-positive microglia were applied on top of the astrocyte layer, co-cultured for one to two weeks, then co-cultures were treated with 4-hydroxytamoxifen for 72 h. The composition of astrocyte–microglia co-cultures was confirmed using co-immunostaining with GFAP and Iba1.

Astrocytes-neuronal co-culture

Neuron-astrocyte co-cultures were prepared by plating neurons onto the astrocyte-feeder layer, as previously described [37]. Briefly, primary astrocytes were cultured on PDL, and laminin coated coverslips/chamber slides for one week. Then, cells were treated with cytosine arabinoside (2.5 µM) for 24 h to arrest the growth of the dividing cells, followed by treatment with 4-hydroxytamoxifen or a mock solution prepared in fresh media for 72 h. One day prior to plating neuronal cells (9–10 day in vitro), the media in astrocyte cultures was replaced with the fresh co-culture media containing 50% astrocytic and 50% neuronal growth media. Then, a cell suspension of the primary mouse cortical neurons (#A15586, ThermoFisher Scientific) was added at a density of 20,000 cells per well to the astrocytes and co-cultured in the 50%/50% media for another 10–12 days. Half of the culture medium was changed every second day.

Cell viability assay

To assess the viability of astrocytes, an MTT (3-(4,5-dimethylthiazol-2-yl)-2,5-diphenyltetrazolium bromide) assay was performed per manufacturer protocol. Briefly, primary astrocytes were seeded in PLL-coated 96-well culture plates at a density of 1 × 10⁴/0.32 cm² in triplicates, then grown until 70–80% confluency and were treated with mock solution or TAM for up to 72 h. The culture medium was cautiously aspirated, then MTT was added and incubated at 37 °C for 4 h in a 5% CO₂ incubator. After adding 100 µl per well of detergent reagent, the plate was kept for 2 h in the dark at room temperature, then absorbance was measured at 570 nm using a Microplate reader (Tecan, infinite 200 PRO, Switzerland).

Preparation of conditioned media

To obtain astrocyte- or microglia-conditioned media, primary astrocytes or microglia were plated at a cell density

of 7×10^5 per culture flask and cultured in a humidified CO₂ incubator at 37°C as described above. After 70–80% confluency (2–3 weeks), media was collected and centrifuged at 1000 rpm for 5 min to remove cellular debris and used immediately.

Protein extraction and Western blotting

Primary astrocytes, astrocytes-microglia co-culture and astrocytes-neuronal co-culture cells were washed with the PBS and homogenized using cell lysis buffer containing a protease inhibitor cocktail. The lysates were centrifuged (4 °C, 20000 g) for 30 min. The protein concentration of each sample was determined using BCA assay, as per the manufacturer's instruction. Protein samples for blotting were prepared with 1X SDS sample loading buffer, and denatured at 85°C for 15 min. Equal amounts of protein (20 µg) along with a pre-stained protein ladder were then loaded onto 10-12% tris-glycine polyacrylamide gel and run in 1X MES SDS running buffer solution at 100 V for 1-2 h. Proteins were transferred onto the PVDF membrane at 16 V for 60 min. Blots were washed with TBST (Tris buffer [10mM Tris, pH 8.0, 150mM NaCl and 0.01% Tween 20]) and then blocked with 5% non-fat milk for 2 h at room temperature. Membranes were then washed thrice with TBST and probed overnight with GFAP (1:3000), STAT3 (1:2000), p-STAT3 (1:2000), complement C-3 (1:2000), PSD-95 (1:2000), Synaptophysin (1:2000) and β-actin (1:10,000) antibodies. Membranes were washed three times with TBST and then blots were incubated with HRP-conjugated secondary antibodies for 1.3–2 h. Protein bands on the blots were visualized on an iBright 1500 imaging system (ThermoFischer Scientific, MA) using Supersignal West pico Maximum Sensitivity Substrate. Protein levels were quantified via densitometry using Bio-Rad Quantity One image analysis software (Bio-Rad, Hercules, CA) and normalized relative to the corresponding levels of β-actin.

Immunocytochemistry

Cells cultured in chamber slides or coverslips were fixed in 4% paraformaldehyde for 15 min at room temperature, washed with PBS followed by permeabilization in methanol for 30 min, then again washed with PBS. Cells were blocked with blocking serum (3% BSA + 1% NGS in PBS) for 2 h and then incubated with primary antibodies at the following dilution: GFAP (1:500), STAT3 (1:1000), p-STAT3 (1:1000), complement C-3 (1:500), MAP2 (1:1000), PSD95 (1:500), Synaptophysin (1:1000) and Drebrin (1:1000) overnight at 4°C. Cells were washed with PBS buffer containing 0.1% TWEEN-20, then incubated with a cocktail of secondary antibodies (Alexa Fluor 488 goat anti-mouse IgG, Alexa Fluor 546 goat anti-mouse IgG, Alexa Fluor 488 goat anti-rabbit IgG, Alexa Fluor 546 goat anti-rabbit IgG, Alexa Fluor

488 goat anti-chicken and Alexa Fluor 647 goat anti-mouse IgG conjugate, all at 1:500 dilution) for 2 h. Cells were then washed with PBS and mounted in VECTA-SHIELD mounting medium with DAPI (Vector Laboratories, Burlingame, CA). Photomicrographic images of the cells were captured using an inverted Nikon Eclipse TE2000-U microscope (Nikon Instech Co. Ltd., Kawasaki, Kanagawa, Japan) or Leica confocal microscope SP8 (Leica Microsystems Inc., Buffalo Grove, IL), and the NIS-Elements microscope imaging software (Nikon Instech Co.) or Leica LAS X software (Leica Microsystems Inc.). Fluorescence integrated intensity was quantified using Image-J 1.42q software (National Institutes of Health, Bethesda, MD).

RT-qPCR

70–80% confluence astrocyte, astrocyte-microglia or neuronal cells cultured on 6-well culture plates (3.0×10^5 cells) were washed with PBS, then total RNA was isolated using the Aurum Mini Kit (Bio Rad, Hercules, CA) according to manufacturer's instruction. The quantity and purity of mRNA were determined using the NanoDrop ND-1000 (ThermoFisher Scientific, Waltham, MA). Complementary DNA (cDNA) synthesis was performed using the iScript cDNA Synthesis Kit as described elsewhere. The cDNA was amplified with a CFX96 Touch Real-Time PCR Detection System (Bio-Rad, Hercules, CA) using SsoAdvanced Universal SYBR Green Supermix. The PCR protocol consisted of incubation at 95 °C for 2 min followed by 40 amplification cycles at 95 °C for 5 s and 60 °C for 30 s. Optimum primer pairs for genes of interest and housekeeping gene, glyceraldehydes 3-phosphate dehydrogenase (Gapdh) were designed using Primer Express version 2.0.0 and PrimerQuest Tool (Table 1). The ΔCt for each RNA sample was calculated by subtracting the mean Ct of the housekeeping gene, Gapdh from the mean Ct of the gene of interest and then relative mRNA gene expression was calculated using the $2^{-\Delta\Delta C_t}$ method as described elsewhere.

Proteome profiler mouse cytokine array

Inflammatory proteins and peptides were quantified using the Proteome Profiler Mouse Cytokine Array Kit, Panel A (#ARY006, R&D Systems) per manufacturer's instructions. In brief, the reconstituted mouse cytokine detection antibody cocktail was mixed with the conditioned media, then added onto the membranes precoated with capture antibodies and incubated overnight at 4 °C on a shaker. Following three washes with wash buffer, the membranes were incubated with Streptavidin-HRP for 30 min at room temperature. After an additional three washes with wash buffer, 1 mL of Chemi Reagent Mix was applied to the membranes for 1 min. The immunoblotted cytokines were visualized using the iBright

Table 1 Primer sequences for qRT-PCR

Primer	Accession number	Sequence
Lcn2	NM_008491.1	F 5'- CCCCATCTCTGCTCACTGTC-3' R 5'- TTTTCTGGACCGCATTG-3'
Serpina3n	NM_009252.2	F 5'- GCAACACCCTGGAAGAGATT-3' R 5'- CTGGTCTGTTTCTCACATAG-3'
Steap4	NM_054098.3	F 5'- CCCGAATCGTGTCTTCTCTATAA-3' R 5'- CCTCGATAGAGCTGCAGAATG-3'
Cxcl10	NM_021274.2	F 5'- AGTAACTGCCGAAGCAAGAA-3' R 5'- GCACCTCCACATAGCTTACA-3'
Serping1	NM_009776.3	F 5'- TGATGGCGCCTTCTTCTAC-3' R 5'- CCACCTTGGCCTTCAAAGTA-3'
S100a10	NM_009112.2	F 5'- GGGCTTCCAGAGCTTCTATC-3' R 5'- CTCAGTTGGCCTACTTCTTC-3'
syp	NM_009305.2	F 5'- CAAGGCTACGGCCAACAG-3' R 5'- GTCTTCGTGGGCTTCACTG-3'
Syn2	NM_001111015.1	F 5'- CCAATCACCAGAGATGCTTAC-3' R 5'- CAATGCTCTGGAAGTCGTAGTG-3'
Dlg4	NM_007864.3	F 5'- CGCTACCAAGATGAAGACACG-3' R 5'- CAATCACAGGGGAGAATTG-3'
Thbs2	NM_011581.3	F 5'- GAACCAACCCTTCGGTGT-3' R 5'- TGGATTCTCTGGCTCACACA-3'
Stat3	NM_213659.3	F 5'- GTGCAGATCATATGGGCTAAA-3' R 5'- CTCAGCACCTTACCCTTATT-3'
Gapdh	NM_001289726.1	F 5'- AACAGCAACTCCCACTCTTC-3' R 5'- CCTGTTGCTGTAGCCGTATT-3'

1500 imaging system (ThermoFischer scientific, MA) and quantified using the Quantity One Image Lab software (Bio-Rad).

Analysis of astrocytes morphology

For identifying the area, perimeter and number of processes in astrocytes, images of non-overlapping GFAP-positive astrocytes were taken using an inverted Nikon Eclipse TE2000-U microscope and analyzed using ImageJ software. Images of 5 random fields of view were selected per well of chamber slides and approximately 15 to 20 images per chamber slide per one experimental condition were taken. After background subtraction and threshold adjusting, 5–6 non-overlapping cells per field of view were analyzed.

Synaptic puncta quantification

Synapse quantification was calculated using custom-written plugin, Puncta Analyzer as described before [38]. Briefly, cells in co-cultured neurons were fixed in 4% PFA and co-immunostained for synaptophysin (SYP), PSD-95 and MAP2. Confocal images were taken using a Leica confocal microscope SP8 (Leica Microsystems Inc.), 63X oil-immersion objective lens at 1024 × 1024 pixel resolution 2X zoom and zoom factor 1.5 corresponding to a voxel dimension 0.13 μm × 0.13 μm × 0.32 μm in X, Y, and Z planes. Cell bodies were centred in the field of view and Z-stack dimensions were set manually by tracking

MAP2-positive neurons including dendrites and soma. Synapses were quantified by analyzing co-localization of SYP and PSD-95 puncta using a custom based plugin Puncta Analyzer in ImageJ. Background was removed separately from the red and green channels using the rolling ball background subtraction algorithm, then thresholding was performed for detecting discrete puncta, and puncta were identified in red and green channels using the Puncta Analyzer plugin. Co-localized puncta were counted as a synapse.

Dendritic spine analysis

Cells in co-cultured neurons were fixed in 4% PFA and co-immunostained for Drebrin and MAP2. Confocal images were taken using a Leica confocal microscope SP8. Images were analyzed using Imaris software (Bitplane, Zurich, Switzerland). Dendritic spine densities were calculated by quantifying the number of spines per 10 μm length of dendritic segments.

Statistics

Statistical analyses were performed with GraphPad PRISM software (GraphPad software, Inc., MA). Comparisons between two groups of independent samples were made with two-tailed, unpaired Student t-tests. Comparisons between multiple groups were made with one-way Anova with Bonferroni multiple comparisons test.

Results

Tamoxifen treatment diminishes Stat3 and phosphorylated Stat3 (p-Stat3) levels in reactive astrocytes isolated from prion-infected mice

To isolate astrocytes, we utilized heterozygous (Aldh1l1-CreERT)^{+/-}-(Stat3-floxP)^{+/+} mice (designated as Cre^{+/-}) as the experimental group and homozygous (Aldh1l1-CreERT)^{-/-}-(Stat3-floxP)^{+/+} mice (designated as Cre^{-/-}) as the negative control. Treatment with 4-hydroxytamoxifen (TAM) is expected to selectively knock out Stat3 in astrocytes derived from Cre^{+/-} mice but not Cre^{-/-} mice. Both groups were infected with the mouse-adapted prion strain 22L via intraperitoneal injection and euthanized at the terminal stage of the disease (140–160 days post-inoculation).

Primary cortical astrocytes were acutely isolated using anti-ACSA-2 microbeads through Magnetic Activated Cell Sorting (MACS) and subsequently cultured in a serum-free medium. A pilot study evaluating TAM toxicity revealed that a concentration of 1 μM had a minor impact on astrocyte viability (Figure S1), while effectively reducing Stat3 expression (Fig. 1A). Additionally, using astrocytes from adult non-infected Cre^{+/-} and Cre^{-/-} mice, we found that TAM treatment did not alter astrocyte morphology, as assessed by cell area, perimeter,

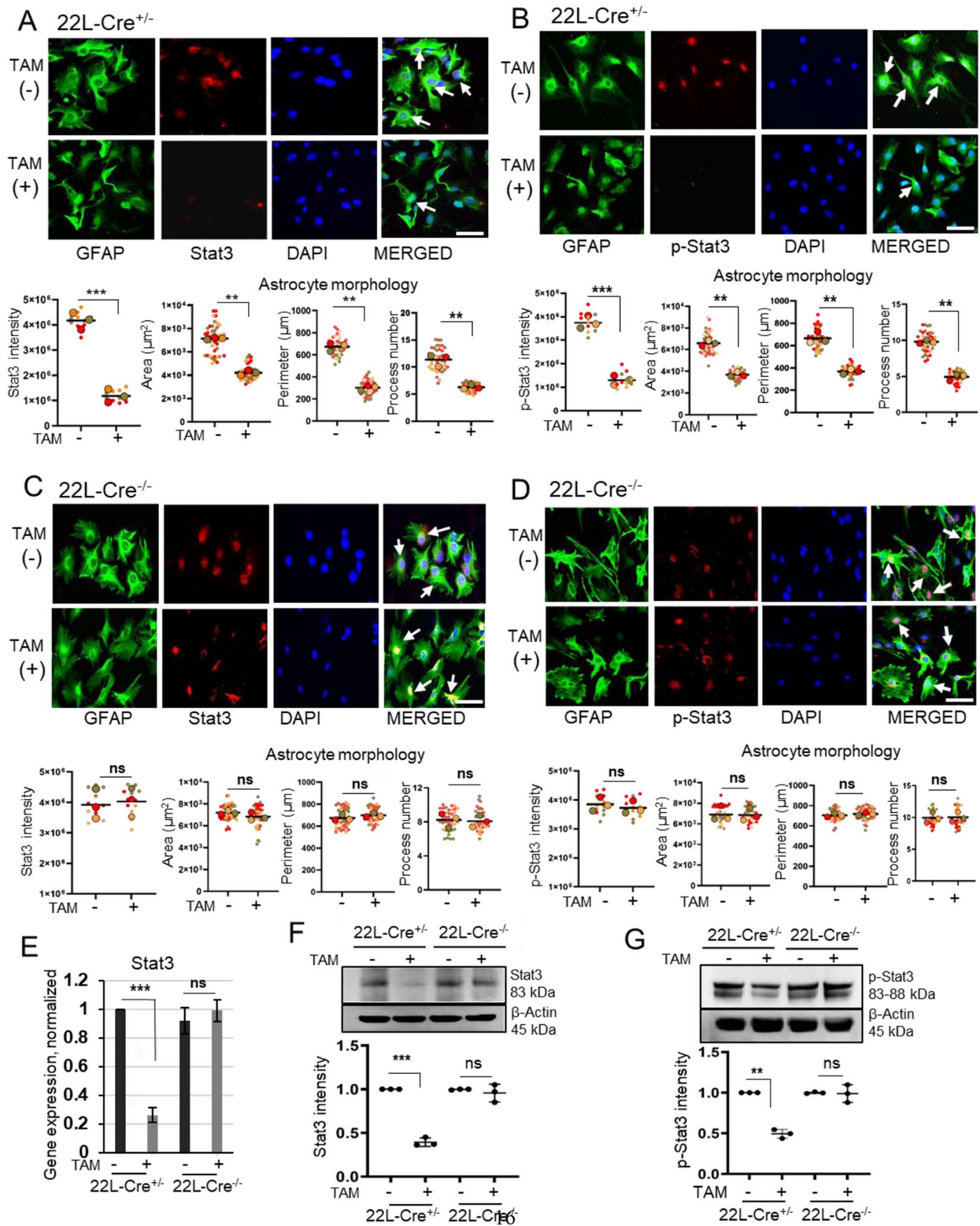


Fig. 1 (See legend on next page.)

(See figure on previous page.)

Fig. 1 Tamoxifen treatment reduces the levels of Stat3 and p-Stat3 in reactive astrocytes isolated from prion-infected mice. Primary astrocytes were treated with TAM or mock solution for 72 h and analyzed. A, B. Upper panels: immunofluorescence microscopy images of 22L-Cre^{+/-} astrocytes co-immunostained for GFAP and Stat3 (A) or p-Stat3 (B) along with DAPI. Lower panels: quantification of integrated fluorescence intensity for Stat3 (A) and p-Stat3 (B), and morphometric analyses of cell area, perimeter and process number in 22L-Cre^{+/-} astrocytes. C, D. Upper panel: immunofluorescence microscopy images of 22L-Cre^{-/-} astrocytes co-immunostained for GFAP and Stat3 (C) or p-Stat3 (D) along with DAPI. Lower panels: quantification of integrated fluorescence intensity for Stat3 (C) or p-Stat3 (D), and morphometric analyses of cell area, perimeter and process number in 22L-Cre^{-/-} astrocytes. Images are representatives of three cultures originating from independent animals per experimental group. For Stat3 or p-Stat3 intensity, $n = 10-12$ random fields with 6-7 cells per field of view from $N = 3$ independent cultures, each prepared from an individual animal, per group. For morphology analysis, $n = 80-100$ cells from $N = 3$ independent cultures, each prepared from an individual animal, per group. In A-D SuperPlots: colors represent independent experiments; dots represent in individual fields of view or cells; average values for each experiment are shown as large circles; statistical analyses were performed based on the number of independent experiments; black lines mark means. E. Analysis of expression of *Stat3* in 22L-Cre^{+/-} and 22L-Cre^{-/-} astrocytes normalized by the expression levels in mock-treated 22L-Cre^{+/-} or 22L-Cre^{-/-} astrocytes using qRT-PCR. F, G. Representative Western blots and densitometric analysis of Stat3 (F) and p-Stat3 (G) expression in 22L-Cre^{+/-} and 22L-Cre^{-/-} astrocytes normalized per expression of β -actin. For E-G, $N = 3$ independent cultures, each prepared from an individual animal, per group. For A-G, N data represent means \pm SE, *** $p < 0.001$, ** $p < 0.01$, and 'ns' non-significant by two-tailed, unpaired t-test, $n = 3$ independent experiments. Scale bar = 50 μ m

and process number (Figure S2A, B). In homeostatic astrocytes, Stat3 is expressed at low levels, and its basal expression remained unchanged upon TAM treatment in both Cre^{+/-} and Cre^{-/-} astrocytes (Figure S2A, B). Based on these findings, the optimized protocol involved a single 1 μ M TAM treatment of astrocytes in cultures.

In agreement with our previous findings on reactive astrocytes derived from 22L-infected C57Bl/6J mice [24], astrocytes isolated from 22L-infected Cre^{+/-} (22L-Cre^{+/-}) and Cre^{-/-} (22L-Cre^{-/-}) mice exhibited hypertrophic morphology (Fig. 1A-D). However, TAM treatment attenuated this hypertrophic morphology, a hallmark of reactive astrocytes, in 22L-Cre^{+/-} astrocytes but not in 22L-Cre^{-/-} astrocytes (Fig. 1A-D). Quantitative analysis of cell area, perimeter, and process number confirmed that TAM reversed the hypertrophic morphology in 22L-Cre^{+/-} astrocytes, while 22L-Cre^{-/-} astrocytes remained unaffected (Fig. 1A-D). Immunostaining revealed significantly reduced levels of Stat3 and its active phosphorylated form, p-Stat3, in TAM-treated 22L-Cre^{+/-} astrocytes compared to their mock-treated counterparts (Fig. 1A, B). As anticipated, TAM treatment did not alter Stat3 or p-Stat3 levels in 22L-Cre^{-/-} astrocytes (Fig. 1C, D).

RT-qPCR and Western blot analyses further confirmed a marked reduction in Stat3 expression at both mRNA and protein levels in TAM-treated 22L-Cre^{+/-} astrocytes relative to mock-treated controls (Fig. 1E, F). Similarly, TAM treatment led to a decrease in p-Stat3 levels in 22L-Cre^{+/-} astrocytes (Fig. 1G). In contrast, Stat3 and p-Stat3 levels remained elevated in TAM-treated 22L-Cre^{-/-} astrocytes (Fig. 1E-G). In summary, Stat3 knockout was confined to astrocytes from Cre^{+/-} mice, confirming the specificity of TAM-induced recombination. While treatment effectively reduced Stat3 and p-Stat3 levels, the knockout efficiency was less than 100%.

Stat3 deletion mitigates reactive phenotype of astrocytes

In prion diseases, astrocytes are known to adopt a reactive C3⁺ phenotype, characterized by the upregulation of

PAN-specific markers *Lcn2*, *Serpina3n*, *Steap4*, *Cxcl10*, alongside A1- and A2-specific markers *Serping1* and *SI100a10*, respectively [20, 39, 40]. Therefore next, we investigated whether Stat3 deletion mitigates this reactive phenotype. Treatment of 22L-Cre^{+/-} astrocytes with TAM resulted in a marked reduction in the mRNA and protein levels of Glial fibrillary acidic protein (GFAP) and C3, compared to mock-treated controls (Fig. 2A, B). Furthermore, the expression levels of *Lcn2*, *Serpina3n*, *Steap4*, *Cxcl10* and *Serping1*, which are indicative of astrocyte reactivity, were significantly decreased in TAM-treated 22L-Cre^{+/-} astrocytes relative to mock-treated cells (Fig. 2C). Conversely, 22L-Cre^{-/-} astrocytes exhibited no response to TAM treatment, as evidenced by unchanged mRNA and protein levels of GFAP and C3, as well as consistent expression of astrocyte reactivity markers (Fig. 2A, B, D). Immunostaining confirmed that cellular C3 levels were significantly reduced in TAM-treated 22L-Cre^{+/-} astrocytes, whereas TAM treatment had no effect on C3 levels in 22L-Cre^{-/-} astrocytes (Fig. 2E, F). In summary, Stat3 depletion effectively reversed the C3⁺ reactive phenotype of astrocytes isolated from prion-infected mice.

Stat3 deficiency partially alleviates the synaptotoxic effects of reactive astrocytes isolated from prion-infected animals

Previously, we demonstrated that reactive astrocytes from prion-infected mice exerted deleterious effects on neurons, including a reduction in dendritic spine density and a loss of synaptic integrity [24]. To assess whether these detrimental effects could be mitigated by reversing astrocyte reactivity, 22L-Cre^{+/-} astrocytes pretreated with TAM were co-cultured with primary neurons.

As expected, neurons co-cultured with 22L-Cre^{+/-} astrocytes exhibited a significant reduction in the colocalization of pre- and postsynaptic proteins, synaptophysin (SYP) and PSD95, respectively, compared to neurons grown with control Cre^{+/-} astrocytes (Fig. 3A). Additionally, the expression of pre-synaptic genes (*Syp*,

Syn2) and the post-synaptic gene *Dlg4* (encoding Discs Large Homolog 4, also known as PSD95) was significantly downregulated in neuronal co-cultures with 22L-Cre^{+/-} astrocytes compared to co-cultures with control astrocytes (Fig. 3B). Consistent with these findings, Western blot analysis revealed substantially lower levels of synaptophysin and PSD95 proteins in neuronal co-cultures with 22L-Cre^{+/-} astrocytes (Figs. 3C, D). Furthermore, spine density was reduced in neurons grown with 22L-Cre^{+/-} astrocytes relative to control co-cultures (Fig. 3E). However, astrocyte-specific deletion of Stat3 partially restored colocalization of pre- and postsynaptic proteins, improved dendritic spine density, elevated the expression of *Syp*, *Syn2*, *Dlg4* and *Thbs2* genes and synaptophysin and PSD95 protein levels in neuronal - astrocyte co-cultures (Figs. 3A–E).

To determine whether the limited recovery was due to incomplete Stat3 deletion, we compared *Stat3* expression levels in TAM-treated 22L-Cre^{+/-} astrocytes, mock-treated 22L-Cre^{+/-} astrocytes, and astrocytes from adult, non-infected Cre^{+/-} mice. As expected, TAM treatment significantly reduced Stat3 expression in 22L-Cre^{+/-} astrocytes relative to mock-treated astrocytes. However, Stat3 expression in TAM-treated astrocytes remained elevated compared to that in non-infected control astrocytes (Fig. 3F). These findings suggest that the limited recovery observed is likely due to the partial efficiency of Stat3 deletion.

Astrocyte-specific Stat3 deletion reverses reactive microglia-induced astrocyte reactivity

Reactive microglia from prion-infected mice have previously been shown to induce a reactive phenotype in astrocytes isolated from non-infected mice [24]. To investigate whether microglia-induced astrocyte reactivity is mediated via a Stat3-dependent pathway, reactive microglia were acutely isolated from 22L-infected mice using CD11b microbeads (referred to hereafter as 22L microglia) and co-cultured with astrocytes isolated from adult, non-infected Cre^{+/-} mice (Fig. 4A). Co-culturing with 22L microglia significantly elevated the cellular levels of Stat3 and its phosphorylated form p-Stat3, in astrocytes compared to Cre^{+/-} astrocytes cultured without reactive microglia (Fig. 4A, E). In parallel with the increased Stat3 and p-Stat3 levels, Cre^{+/-} astrocytes co-cultured with 22L microglia exhibited hypertrophic morphology, characterized by increased cell area, perimeter, and process number (Fig. 4A, E).

Treatment with TAM effectively reversed the upregulation of Stat3 and p-Stat3 in Cre^{+/-} astrocytes co-cultured with 22L microglia (Fig. 4A, E). Western blot analysis confirmed significantly lower levels of Stat3 and p-Stat3 in TAM-treated Cre^{+/-} astrocytes co-cultured with 22L microglia compared to mock-treated counterparts under

the same co-culture conditions (Fig. 4B, F). Importantly, partial loss of Stat3 and the concurrent depletion of p-Stat3 reversed, to a large extent, the astrocyte reactive phenotype characterized by hypertrophic morphology (Fig. 4A, E). Furthermore, Stat3 and p-Stat3 deficiency reversed the upregulation of astrocyte reactivity markers, including GFAP, as quantified by Western blotting, and *Lcn2*, *Serpina3n*, *Steap4*, *Cxcl10* and *Serping1*, as assessed by RT-qPCR (Fig. 4C, D). In summary, Stat3 deletion in astrocytes and the subsequent depletion of its activated form p-Stat3 reversed the phenotypic transition of astrocytes to a pro-inflammatory, reactive state.

Microglia-secreted factors are responsible for Stat3-dependent astrocyte reactivity

To assess whether Stat3-dependent astrocyte reactivity is induced by factors secreted by microglia, we evaluated the effects of medium conditioned by 22L reactive microglia (22L MCM) on astrocytes isolated from adult non-infected Cre^{+/-} mice. Cre^{+/-} astrocytes treated with 22L MCM showed a significant upregulation of both cellular Stat3 and p-Stat3 compared to those cultured without 22L MCM (Fig. 5A, D). Similar to Cre^{+/-} astrocytes co-cultured with 22L microglia, exposure to 22L MCM induced hypertrophic morphology in Cre^{+/-} astrocytes, characterized by increased cell area, cell perimeter, and a greater number of processes (Fig. 5A, D).

Tamoxifen treatment largely prevented the upregulation of Stat3 and p-Stat3 in Cre^{+/-} astrocytes cultured with 22L MCM (Fig. 5A, D). Western blot analysis confirmed significantly lower levels of Stat3 and p-Stat3 in tamoxifen-treated versus mock-treated Cre^{+/-} astrocytes (Fig. 5B, E). The loss of Stat3 and corresponding depletion of p-Stat3 largely prevented the phenotypic transition to a hypertrophic morphology (Fig. 5A, D). Furthermore, the loss of Stat3/p-Stat3 signaling prevented the upregulation of reactive astrocyte markers *Lcn2*, *Serpina3n*, *Steap4*, *Cxcl10* and *Serping1* in Cre^{+/-} astrocytes cultured with 22L MCM (Fig. 5C). These findings demonstrate that factors secreted by reactive microglia drive Stat3-mediated astrocyte reactivity.

Both reactive microglia and astrocytes in prion-infected animals secrete pro-inflammatory factors including IL-6

Previous studies have reported the upregulation of multiple genes associated with pro-inflammatory phenotypes in reactive microglia and astrocytes in the context of prion diseases [19–21, 23, 41]. However, upregulation of inflammatory molecules at the protein level has not been documented. To identify inflammatory proteins and peptides, a mouse cytokine array that profiles 40 molecules was applied to reactive microglia and astrocytes acutely isolated from 22L-infected mice (Figure S3).

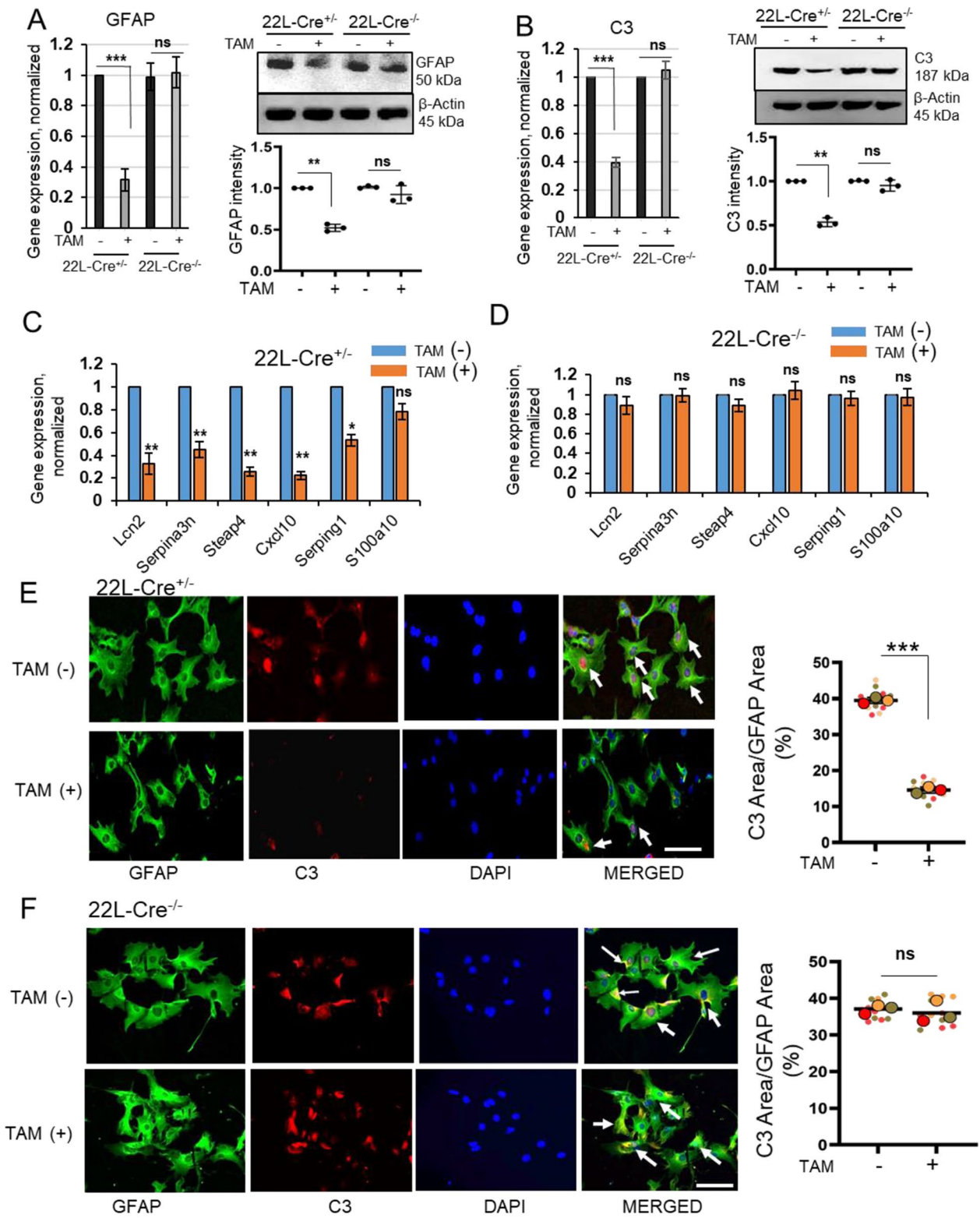


Fig. 2 (See legend on next page.)

(See figure on previous page.)

Fig. 2 Stat3 deletion mitigates the reactive phenotype of astrocytes isolated from prion-infected mice. Primary astrocytes were treated with TAM or mock solution for 72 h and analyzed. **A, B.** Left panels: analysis of *GFAP* (**A**) and *C3* (**B**) gene expression in 22L-Cre^{+/−} and 22L-Cre^{−/−} astrocytes using qRT-PCR. Right panels: representative Western blots and densitometric analysis of *GFAP* (**A**) and *C3* (**B**) expression normalized per expression of β -actin in 22L-Cre^{+/−} and 22L-Cre^{−/−} astrocytes. **C, D.** Analysis of expression of genes associated with astrocyte reactivity in 22L-Cre^{+/−} (**C**) and 22L-Cre^{−/−} (**D**) astrocytes. The expression levels in TAM-treated astrocytes were normalized relative to those in mock-treated astrocytes. In **A–D**, $N=3$ independent cultures, each prepared from an individual animal, per group. Data represent means \pm SE, $***p < 0.001$, $**p < 0.01$, $*p < 0.05$ and 'ns' is non-significant by two-tailed, unpaired t -test. **E, F.** Left panels: immunofluorescence microscopy images of 22L-Cre^{+/−} (**E**) and 22L-Cre^{−/−} (**F**) astrocytes co-immunostained for *GFAP* and *C3* along with DAPI. Right panels: quantification of the *C3*-positive area within *GFAP*-positive 22L-Cre^{+/−} (**E**) and 22L-Cre^{−/−} (**F**) astrocytes. Images are representatives of three cultures originating from independent animals. $n = 13$ random fields with 8–10 cells per field of view from $N = 3$ independent cultures, each prepared from an individual animal, per group. In **E** and **F** SuperPlots: colors represent independent experiments; dots represent in individual fields of view; average values for each experiment are shown as large circles; statistical analyses were performed based on the number of independent experiments; black lines mark means, $***p < 0.001$, 'ns' is non-significant by two-tailed, unpaired t -test. Scale bar = 50 μ m

In the culture media from reactive microglia, we observed a significant upregulation of pro-inflammatory cytokines IL-1 α , IL-1 β , and TNF- α , as well as pro-inflammatory chemokines CCL3, CCL5, and CXCL10 (Fig. 6A, C; Table 2). Additionally, the anti-inflammatory cytokine IL-1ra (interleukin-1 receptor antagonist) was upregulated, alongside a downregulation of ICAM-1 (intercellular adhesion molecule 1) (Fig. 6A, C). Among the molecules secreted by reactive astrocytes, cytokine IL-12 and chemokines CCL4, CCL12, and CXCL12 were significantly upregulated, while TIMP-1 (tissue inhibitor of metalloproteinase-1), a glycoprotein involved in neuroprotection [42, 43], was downregulated (Fig. 6B, C; Table 2).

Notably, both reactive microglia and astrocytes exhibited elevated levels of the pro-inflammatory cytokine IL-6 and chemokines CCL2 and CXCL1 (Fig. 6C, D). These findings suggest that both reactive microglia and astrocytes contribute to the upregulation of overlapping subsets of secreted inflammatory molecules (Fig. 6D). Among the factors strongly upregulated by both cell types, IL-6 stands out as a key molecule known to activate the JAK2/Stat3 signaling pathway [44–46].

IL-6 induces astrocyte reactivity in a Stat3-dependent manner

To investigate the role of IL-6 in astrocyte activation, cellular levels of Stat3, p-Stat3, *GFAP*, and *C3* were analyzed in astrocytes isolated from adult, non-infected Cre^{+/−} mice and treated with recombinant IL-6 using Western blotting. Stat3, p-Stat3, *GFAP*, and *C3* levels were significantly elevated in IL-6-treated astrocytes compared to mock-treated controls (Fig. 7A). Furthermore, IL-6 treatment increased the expression of the markers associated with astrocyte reactivity in prion disease *Lcn2*, *Serpina3n*, *Steap4*, *Cxcl10*, *Serping1*, and *S100a10* (Fig. 7B). Notably, pretreatment of Cre^{+/−} astrocytes with tamoxifen attenuated IL-6-induced astrocyte reactivity. This attenuation was evidenced by reduced cellular levels of Stat3, p-Stat3, *GFAP*, and *C3*, as well as decreased expression of *Lcn2*, *Serpina3n*, *Steap4*, *Cxcl10*, *Serping1*, and *S100a10* (Fig. 7A, B). In summary, exposure of normal

astrocytes to IL-6 alone is sufficient to induce astrocyte reactivity via a Stat3-dependent mechanism.

Discussion

In a healthy brain, astrocytes play essential physiological roles tailored to specific neuronal subpopulations and brain regions [47–49]. Under normal conditions, astrocytes demonstrate distinct regional homeostatic identities, adapting to the unique demands of their local environment [19]. Notably, seven developmentally predetermined astrocyte subtypes have been identified in different regions of the mouse brain [50]. However, in neurodegenerative conditions, including prion diseases, astrocytes adopt reactive phenotypes that persist throughout disease progression [1, 2, 18, 21–23].

In chronic neurodegenerative diseases such as prion diseases, astrocyte reactivity initially arises as a physiological response to an altered brain environment. However, prolonged exposure to prion infection leads to the emergence of a disease-associated astrocytic phenotype, which disrupts their homeostatic functions. Transcriptomic analyses of prion-infected animals have revealed widespread disturbances in astrocyte-specific genes involved in diverse functions, including BBB regulation, transporters, myelination, energy metabolism, extracellular matrix remodeling, growth factor signaling, and neuroprotection [19, 23]. Notably, genes critical for synapse formation and maintenance, such as *Nrxn1*, *Nlgn1*, *Cdh10*, *Gpc4*, and *Gpc5*, were markedly downregulated, reflecting a loss of neuronal support functions [19]. In contrast, the strong upregulation of *C3*, a gene associated with a neurotoxic astrocyte phenotype, was consistently observed in reactive astrocytes in prion diseases [24, 26, 40, 51, 52]. Interestingly, *C3* upregulation has been identified as a universal marker of neurotoxic astrocytes across multiple neurological conditions, underscoring its relevance to astrocyte-mediated neurotoxicity [53–56]. In prion diseases, reactive astrocytes exhibited gene signature shared across various prion strains [19].

Functionally, reactive astrocytes isolated from prion-infected animals exerted detrimental effects on primary neuronal cultures, including reduced dendritic spine size

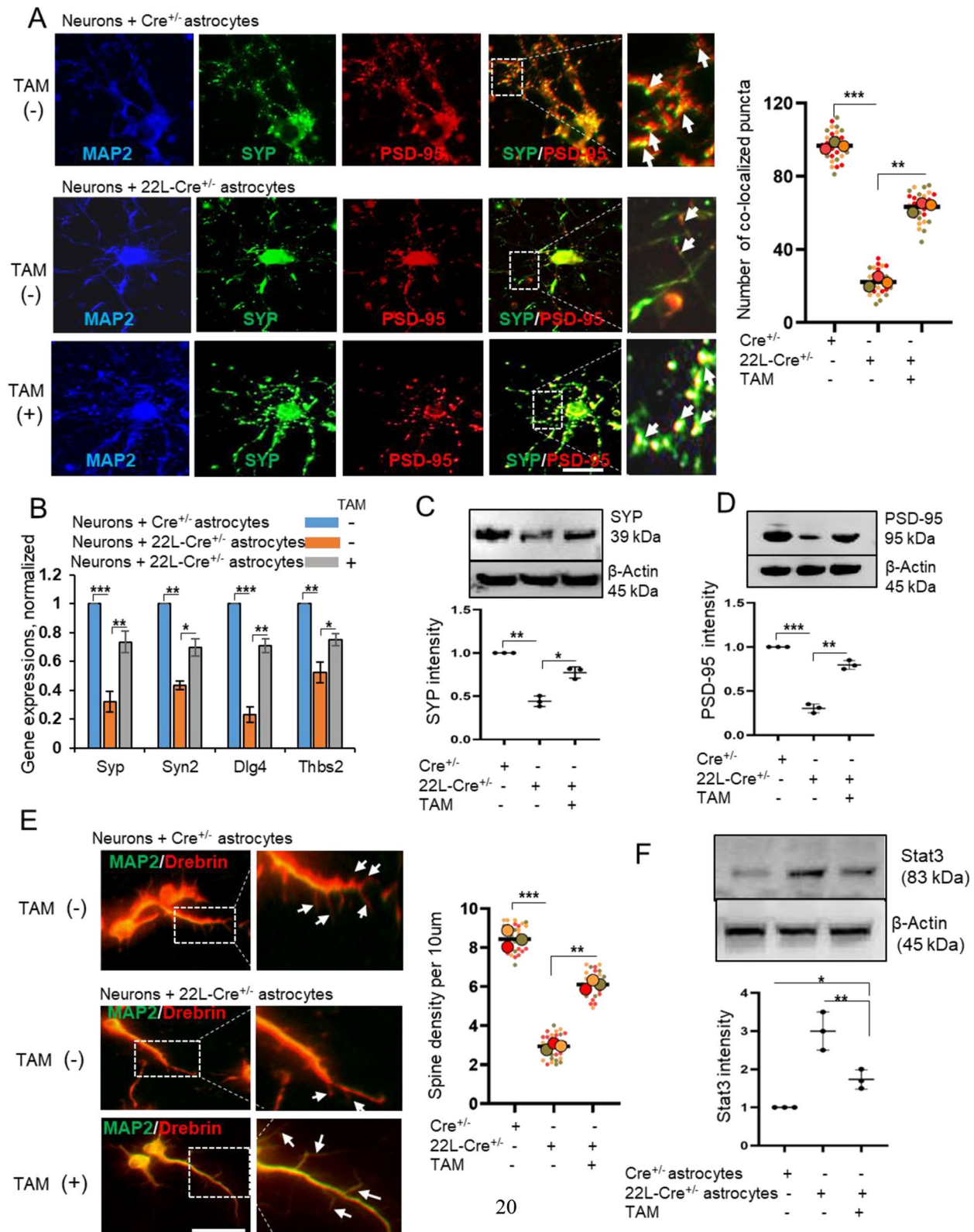


Fig. 3 (See legend on next page.)

(See figure on previous page.)

Fig. 3 Stat3 deletion alleviates the synaptotoxic effects of reactive astrocytes from prion-infected mice. Cre^{+/-}, 22L-Cre^{+/-}, and TAM-pretreated 22L-Cre^{+/-} astrocytes were co-cultured with primary cortical neurons for 10–12 days. 24 h prior of coculturing with neurons, the culture media containing TAM in astrocyte cultures was replaced with the fresh co-culture media without TAM, as described in Methods. **(A)** Left panels: fluorescence microscopy images of cortical neurons co-cultured with Cre^{+/-}, 22L-Cre^{+/-} or TAM-pretreated 22L-Cre^{+/-} astrocytes and co-immunostained for MAP2 and pre- and post-synaptic markers synaptophysin (SYP) and PSD95, respectively. Arrows indicate puncta of co-localized SYP and PSD95. Right panel: quantification of co-localized puncta per field of view in co-cultures. $N=23$ random fields of view with 1–2 neurons per field of view from $N=3$ independent cultures. **(B)** Analysis of expression of *Syp*, *Syn2*, *Dlg4* and *Thbs2* genes in neurons co-cultured with astrocytes using qRT-PCR. **(C, D)** Representative Western blots and densitometric analysis of SYP **(C)** and PSD-95 **(D)** expression normalized per expression of β -actin in co-cultures. **(E)** Left panels: fluorescence microscopy images of cortical neuronal cells co-cultured with Cre^{+/-}, 22L-Cre^{+/-} and TAM-pretreated 22L-Cre^{+/-} astrocytes co-immunostained for spine marker Drebrin and MAP2. Right panel: quantification of spine density in co-cultures. In **(E)**, 30–40 neurons for each experimental condition. In **(A)** and **(E)** SuperPlots: colors represent independent experiments; dots represent in individual fields of view or neurons; average values for each experiment are shown as large circles; statistical analyses were performed based on the number of independent experiments; black lines mark means. **(F)** Representative Western blots and densitometric analysis of Stat3 expression astrocytes from adult, non-infected Cre^{+/-} mice, TAM-treated 22L-Cre^{+/-} astrocytes and mock-treated 22L-Cre^{+/-} astrocytes normalized per expression of β -actin. In **(A–F)**, Data represent means \pm SE, * $p < 0.05$, ** $p < 0.01$, *** $p < 0.001$, by one-way ANOVA with Bonferroni post-hoc test, $N=3$ independent culture experiments per group, each prepared from an individual animal, per group. Scale bars = 25 μ m **(A)** and 10 μ m **(E)**

and density, impaired neuronal growth, and compromised synapse integrity [24]. Additionally, these reactive astrocytes induced a disease-associated phenotype in endothelial cells, impairing BBB integrity [25]. These changes included the disintegration of tight and adherens junctions and reduced trans-endothelial electrical resistance [25]. In prion-infected mice, astrocytic endfeet retraction from blood vessels and loss of BBB integrity were observed even before clinical disease onset, highlighting their early involvement in disease pathogenesis [19, 25].

Whether astrocytic reactive phenotypes can be effectively reversed in vivo has been a topic of ongoing debate. Previous studies on optic nerve injury, induced by brief elevations in ocular pressure, demonstrated that astrocyte reactivity can be fully resolved upon removal of the insult [57]. However, in the context of more severe injuries, such as spinal cord trauma that results in glial scar formation composed of reactive astrocytes, these phenotypic changes were traditionally considered irreversible. Interestingly, recent research has revealed that reactive astrocytes isolated from injured spinal cords can reverse their phenotype when transplanted into a naïve spinal cord [58].

The current study demonstrates that the Stat3 pathway is critical for activating astrocytes in prion diseases and that their reactive phenotype can be reversed by deleting Stat3. Reversing astrocyte reactivity mitigated their synaptotoxic effects. These results align well with recent studies showing that blocking IL-6 signaling prevents astrocyte-induced neuronal death in an induced pluripotent stem cell (iPSC)-based model of Parkinson's disease [59].

To investigate the mechanism underlying astrocyte activation, reactive microglia from prion-infected mice were co-cultured with normal astrocytes. These experiments revealed that astrocyte activation by reactive microglia is mediated through the Stat3 pathway. Moreover, Stat3-dependent activation of astrocytes was recapitulated using media conditioned by reactive microglia,

suggesting that microglia-derived soluble factors drive astrocyte reactivity. Inflammatory protein and peptide profiling demonstrated that in the reactive states, microglia and astrocytes upregulated two partially overlapping subsets of secreted inflammatory molecules. Among these, IL-6, a cytokine known to activate the JAK2/Stat3 pathway [44–46], was prominently upregulated in both reactive microglia and astrocytes. Notably, exposure of normal astrocytes to IL-6 alone was sufficient to upregulate p-Stat3 and induce the C3-positive reactive phenotype. Our findings that IL-6 is secreted by both reactive microglia and astrocytes suggest that astrocyte reactivity can be induced or sustained not only with the help of reactive microglia but also by reactive astrocytes in a self-reinforcing, cell-autonomous manner.

Previous studies have shown that neurotoxic astrocyte reactivity is driven by reactive microglia through the secretion of IL-1 α , TNF- α , and C1q [54]. However, in prion-infected triple knockout mice (Il1 α ^{-/-}, TNF α ^{-/-}, and C1q^{-/-}), only modest changes in the reactive astrocyte phenotype were observed [40]. Unexpectedly, disease progression was accelerated in these knockout mice compared to prion-infected controls, challenging the presumed role of IL-1 α /TNF- α /C1q signaling in driving neurotoxic astrocyte activation in prion diseases [40]. Our findings suggest that an alternative, IL-6-dependent pathway may contribute to astrocyte activation in prion disease.

The findings of this study are consistent with previous research on other neurodegenerative diseases, highlighting the role of the JAK2/Stat3 pathway in astrocyte activation. In the APP/PS1dE9 mouse model of Alzheimer's disease, inhibition of the JAK2/Stat3 pathway via viral vectors was shown to reduce amyloid deposition, improve spatial learning, and restore synaptic deficits [28]. Similarly, conditional deletion of Stat3 in astrocytes in APP/PS1dE9 mice led to a decreased pro-inflammatory cytokine response, reduced A β plaque burden, lowered dystrophic neurite burden, and alleviated memory decline [29]. In contrast, the astrocytic JAK2/Stat3

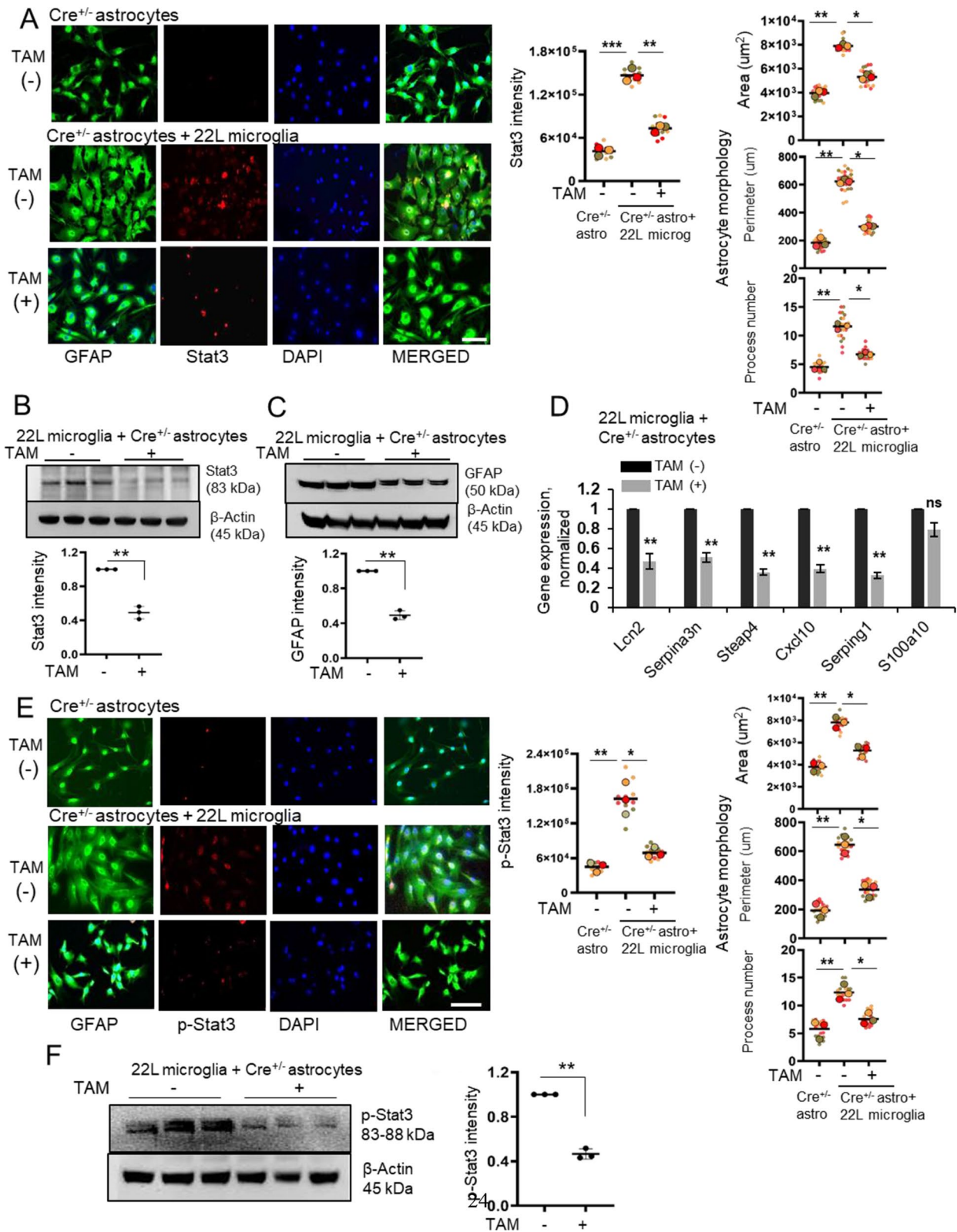


Fig. 4 (See legend on next page.)

(See figure on previous page.)

Fig. 4 Astrocyte-specific deletion of Stat3 reverses microglia-induced astrocyte reactivity. Astrocyte – 22L microglia co-cultures were treated with TAM or mock solution for 72 h and analyzed **A**. Left panels: immunofluorescence microscopy images of Cre^{+/-} astrocytes co-cultured with 22L microglia and co-immunostained for GFAP and Stat3 along with DAPI. Cre^{+/-} astrocytes cultured in the absence of microglia are presented as reference. Right panels: quantification of integrated fluorescence intensity of Stat3, and morphometric analyses of cell area, perimeter and process number of astrocytes. **B, C**. Representative Western blots and densitometric analysis of Stat3 (**B**) and GFAP (**C**) expression normalized per expression of β -actin. **D**. Analysis of expression of genes associated with astrocyte reactivity in Cre^{+/-} astrocytes co-cultured with 22L microglia using qRT-PCR. **E**. Left panels: immunofluorescence microscopy images of Cre^{+/-} astrocytes co-cultured with 22L microglia and co-immunostained for GFAP and p-Stat3 along with DAPI. Cre^{+/-} astrocytes cultured in the absence of microglia are presented as reference. Right panels: quantification of integrated fluorescence intensity of p-Stat3 and morphometric analyses of cell area, perimeter and process number of astrocytes. **F**. Representative Western blots and densitometric analysis of p-Stat3 expression normalized per expression of β -actin. In **A** and **E**, images are representatives of three cultures originating from individual animals; for Stat3 and p-Stat3 intensity, $n = 10$ random fields with 5–7 cells per field from $N = 3$ independent cultures per group; for morphology analysis, $n = 80$ –100 cells from $N = 3$ independent cultures per group. In SuperPlots: colors represent independent experiments; dots represent in individual fields of view or cells; average values for each experiment are shown as large circles; statistical analyses were performed based on the number of independent experiments; black lines mark means. In **B–D** and **F**, $N = 3$ independent cultures, each prepared from an individual animal, per group. In **A–F**, data represent means \pm SE, *** $p < 0.001$, ** $p < 0.01$, * $p < 0.05$, 'ns' is non-significant by one-way ANOVA with Bonferroni multiple comparisons test (in **A** and **E**) and by two-tailed, unpaired t -test (in **B–D** and **F**). Scale bars = 50 μ m

pathway appears to play a protective role in Huntington's disease. Activation of this pathway in astrocytes in mouse models of Huntington's disease reduced the aggregation of mutant Huntingtin in neurons and mitigated neuronal defects [60]. Collectively, these findings indicate that the JAK2/Stat3-modulated reactive astrocyte phenotype may have disease-specific effects, yielding protective or detrimental outcomes depending on the context of the neurodegenerative condition.

Recent studies have highlighted the intricate crosstalk between microglia and astrocytes, revealing a complex interplay mediated through multiple signaling pathways [61, 62]. The reactive states of these glial cells appear to be interdependent, but whether reactive microglia directly induce reactive phenotypes in astrocytes remains an open question. Our previous and current studies demonstrated that reactive microglia isolated from prion-infected mice can drive astrocyte reactivity (23). Intriguingly, microglia depletion in prion-infected mice resulted in an exacerbated C3-positive reactive phenotype in astrocytes, which accelerated disease progression [52, 63–65]. Collectively, these findings suggest that astrocytes can be activated through both microglia-dependent and independent mechanisms. Furthermore, in the absence of microglia, astrocytes may exhibit heightened proinflammatory reactivity, potentially compensating for the loss of reactive microglia.

This study demonstrates that reactive astrocytes associated with prion disease upregulate the secretion of several cytokines, including IL-6, IL-12, CCL2, CCL4, CCL12, CXCL1, and CXCL12. Notably, most of these cytokines, specifically CCL2, CCL4, CCL12, CXCL1, and CXCL12, are linked to pro-inflammatory responses. These cytokines play critical roles in recruiting myeloid cells from the periphery, enhancing BBB permeability, and mediating crosstalk between astrocytes and microglia, ultimately leading to the activation of pro-inflammatory microglia. Chronic neuroinflammation driven by pro-inflammatory cytokines is well-documented to have

adverse effects [66, 67]. In addition to the upregulation of pro-inflammatory cytokines, reactive astrocytes associated with prion disease downregulate TIMP-1 secretion, indicating a loss of essential homeostatic functions. TIMP-1 has been shown to play a neuroprotective role by inhibiting neuronal apoptosis [42, 43]. In AD mouse models, TIMP-1 protected neurons from A β toxicity, restored synaptic plasticity, increased dendritic spine size, and ameliorated A β -induced cognitive dysfunction [43, 68]. Interestingly, IL-12 exhibits context-dependent effects that vary across the disease model. In AD mouse models, IL-12 contributes to a pro-inflammatory response, exacerbating A β plaque pathology. Conversely, in experimental autoimmune encephalomyelitis, IL-12 induces an anti-inflammatory response, promoting neuroprotective adaptations within the CNS [69, 70]. It remains unclear whether the upregulation of the above cytokines in prion diseases arises from the same or different subpopulations of reactive astrocytes.

IL-6 is a pleiotropic cytokine that can exert opposing effects within the CNS, functioning as either anti-inflammatory and neuroprotective or pro-inflammatory and neurotoxic [71, 72]. Notably, upregulation of IL-6 has been observed in various neurological disorders associated with neuroinflammation, including Alzheimer's disease, Parkinson's disease, and multiple sclerosis [73–77]. IL-6 signaling is mediated through both membrane-bound and soluble forms of the IL-6 receptor (IL-6R), enabling it to target multiple CNS cell types in a context-dependent manner [78]. The pro-inflammatory pathway associated with neurodegeneration involves IL-6 binding to the soluble form of IL-6R, which triggers responses in distal cells via a mechanism known as trans-signaling [78]. This trans-signaling is recognized as the predominant mechanism underlying the pathogenic, pro-inflammatory effects of IL-6 in the CNS, as it targets cells that do not express membrane-bound IL-6R [79]. Overexpression of IL-6 under the GFAP promoter in mice has

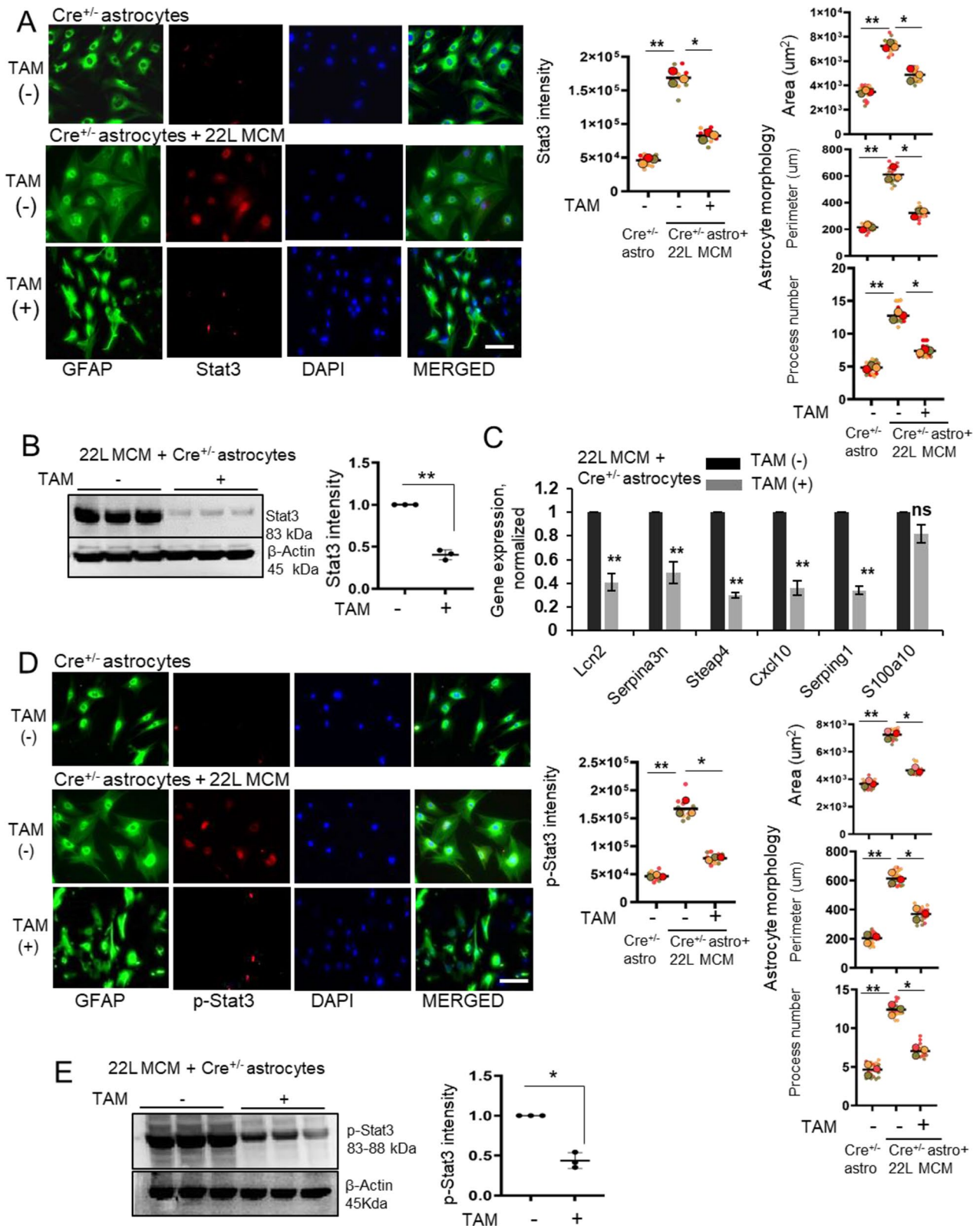


Fig. 5 (See legend on next page.)

(See figure on previous page.)

Fig. 5 Stat3-mediated astrocyte reactivity is induced by microglia-secreted factors. Astrocytes were cultured in the presence of 22L MCM and TAM or mock solution for 72 h and analyzed. **A.** Left panels: immunofluorescence microscopy images of Cre^{+/-} astrocytes co-immunostained for GFAP and Stat3 along with DAPI. Cre^{+/-} astrocytes cultured in the absence of 22L MCM are presented as reference. Right panels: quantification of integrated fluorescence intensity of Stat3, and morphometric analyses of cell area, perimeter and process number of astrocytes. **B.** Representative Western blot and densitometric analysis of Stat3 expression normalized per expression of β -actin. **C.** Analysis of expression of genes associated with astrocyte reactivity in Cre^{+/-} astrocytes cultured in the presence of 22L MCM using qRT-PCR. **D.** Left panels: immunofluorescence microscopy images of Cre^{+/-} astrocytes co-immunostained for GFAP and p-Stat3 along with DAPI. Right panels: quantification of integrated fluorescence intensity of p-Stat3 and morphometric analyses of cell area, perimeter and process number. **E.** Representative Western blots and densitometric analysis of p-Stat3 expression normalized per expression of β -actin. In **A** and **D**, images are representatives of $N=3$ cultures originating from individual animals; for Stat3 and p-Stat3 intensity, $n=10$ random fields with 5–6 cells per field from $N=3$ independent cultures originating from individual animals; for morphology analysis, $n=70$ –80 cells from $N=3$ independent cultures, originating from individual animals. In SuperPlots: colors represent independent experiments; dots represent in individual fields of view or cells; average values for each experiment are shown as large circles; statistical analyses were performed based on the number of independent experiments; black lines mark means. In **B**, **C** and **E**, $N=3$ independent cultures, originating from individual animals. In **A-E**, data represent means \pm SE, ** $p < 0.01$, * $p < 0.05$, 'ns' is non-significant by one-way ANOVA with Bonferroni multiple comparisons test (in **A** and **D**) and by two-tailed, unpaired t-test (in **B**, **C** and **E**). Scale bars = 50 μ m

been shown to induce neurological disease characterized by neurodegeneration and reactive astrogliosis [80].

In the present study, Stat3-dependent astrocyte activation was shown to rely on secreted IL-6. Previously, we demonstrated that PrP^{Sc} directly upregulates IL-6 secretion by microglia [81]. Additionally, our prior work established that IL-6 contributes to pathological changes in endothelial cells and compromises BBB integrity in prion diseases [25]. Here, we observed that IL-6 was significantly upregulated not only in reactive microglia but also in reactive astrocytes isolated from prion-infected mice. These findings suggest that, once activated, the reactive state of astrocytes may no longer depend on non-cell-autonomous stimuli from other cell types. Future studies could explore whether suppressing IL-6 delays disease progression and ameliorates clinical symptoms in prion diseases.

The primary limitation of the present study is that the effects of Stat3 downregulation were assessed only in primary astrocytes isolated from prion-infected mice or in astrocytes co-cultured with neurons, but not in vivo. Whether Stat3 downregulation can mitigate disease progression in prion-infected animals remains under investigation. Approaches based on primary cultures, while informative, do not capture the complex intercellular interactions present within the intact brain and fail to reflect the inherent complexity of disease mechanisms. Relying solely on in vitro models makes it difficult to predict how the strong proinflammatory environment and progressive elevation of PrP^{Sc} levels during disease development might influence the effects of Stat3 downregulation on astrocyte reactivity. Additionally, potential compensatory mechanisms involving redundant pathways, such as those mediated by Stat1 and Stat2, may further modulate the outcomes observed.

Targeting the reactive state of astrocytes in vivo presents several challenges. First, the reactive phenotype of astrocytes, as well as their functional roles, likely evolves with disease progression. Identifying the optimal time window for suppressing astrocyte reactivity is

therefore crucial. Second, astrocyte reactivity exhibits pronounced heterogeneity across disorders [9, 82]. Given that astrocytes are known to display region-specific heterogeneity and region-specific responses to prions [19, 83], achieving desirable manipulation of their reactive phenotype across the entire brain may be particularly challenging. Third, the dynamics of prion invasion and disease progression, both of which vary by brain region, are influenced by the prion strain or specific subtype of Creutzfeldt–Jakob disease. Consequently, astrocytes in affected regions may be at different stages of activation or display distinct reactive phenotypes. Fourth, the interplay between microglia and astrocytes further complicates efforts to modulate astrocyte reactivity. Altering the reactive state of one cell type is likely to influence the other, and the nature of microglia-astrocyte interactions may shift as the disease progresses, posing additional challenges. Finally, the potential upregulation of alternative signaling pathways, such as those mediated by Stat1 and/or Stat2, may serve as compensatory mechanisms. Since Stat1 and Stat2 are expressed in astrocytes and contribute to their activation in response to CNS infections or injury [84, 85], their upregulation could counteract efforts to suppress astrocyte reactivity via Stat3 downregulation, and must be accounted for in therapeutic approaches.

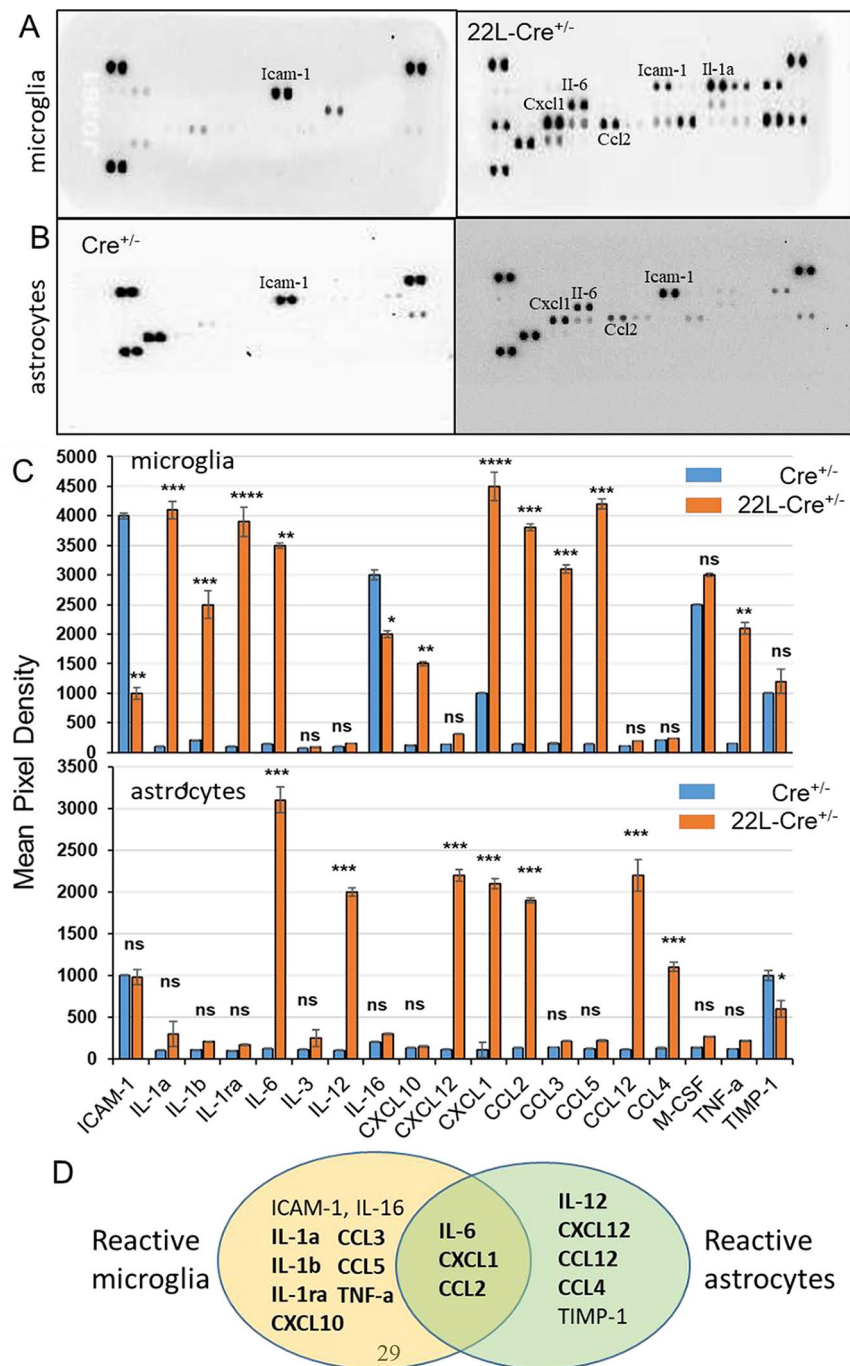


Fig. 6 Reactive microglia and astrocytes secrete pro-inflammatory factors. Analysis of media conditioned by reactive microglia and astrocytes isolated from 22L-Cre^{+/-} and non-infected, adult Cre^{+/-} mice using cytokine/chemokine profiling array. **A, B.** Representative array images of mouse cytokines in media conditioned by reactive microglia (**A**) and astrocytes (**B**). **C.** Quantification cytokines secreted by microglia and astrocytes from 22L-Cre^{+/-} and Cre^{+/-} animals. **D.** Venn diagram illustrating an overlap in secreted molecules between reactive astrocytes and microglia. Factors upregulated or down-regulated in reactive versus homeostatic states are shown using bold and thin fonts, respectively. Data represent mean ± SE, *****p* < 0.0001, ****p* < 0.001, ***p* < 0.01, **p* < 0.05 and 'ns' is non-significant by two-tailed, unpaired *t*-test, N=3 independent experiments, where conditioned media were obtained from three independent cultures, each originating from an individual animal

Table 2 List of factors, secretion of which is up- or down-regulated in reactive States of microglia and astrocytes

Protein	Density		Astrocytes	
	Microglia		normal	reactive
	normal	reactive	normal	reactive
ICAM-1	4033 ± 88*	1005 ± 80	1009 ± 5.5	993 ± 58
IL-1a	105 ± 6	4133 ± 145	105 ± 4.4	301 ± 57
IL-1b	200 ± 5.8	2533 ± 260	107 ± 4.7	205 ± 3.8
IL-1ra	103 ± 6.7	3900 ± 295	96 ± 7.2	169 ± 11
IL-6	140 ± 5.4	3511 ± 119	120 ± 2.9	3121 ± 104
IL-12	105 ± 5.8	155 ± 7.6	103 ± 5.8	2047 ± 33
IL-16	3033 ± 202	1993 ± 121	201 ± 15	305 ± 15
CXCL10	121 ± 2.6	1507 ± 57	130 ± 5.8	153 ± 6.1
CXCL12	136 ± 6.0	317 ± 11.9	110 ± 6.2	2200 ± 57
CXCL1	1026 ± 17	4512 ± 261	113 ± 21	2133 ± 88
CCL2	139 ± 5.9	3834 ± 88	135 ± 7.6	1932 ± 33
CCL3	151 ± 10	3153 ± 129	141 ± 4.5	210 ± 11
CCL5	140 ± 5.8	4241 ± 83	121 ± 7.3	216 ± 3.2
CCL12	111 ± 3.7	190 ± 5.6	111 ± 8.7	2217 ± 124
CCL4	210 ± 5.7	234 ± 8.6	131 ± 6.0	1099 ± 57
TNF-α	153 ± 5.5	2111 ± 57	116 ± 2.9	213 ± 2.6
TIMP-1	1007 ± 8.8	1196 ± 98	1003 ± 54	613 ± 40

* Bold font used for secreted factors that were found to be up- or downregulated in reactive states relative to homeostatic states with high statistical significance

Abbreviations

22L Mouse adapted prion strain
AD Alzheimer's Disease

Aldh111 Aldehyde dehydrogenase 1 family member L1
BBB Blood brain barrier
C3 Complement component 3 protein
CNS Central Nervous System
Dlg4 Discs Large Homolog 4, also known as PSD95
GFAP Glial fibrillary acidic protein
JAK2 Janus Kinase 2
IL-6 Interleukin-6
IL-6R IL-6 receptor
i.p. Intraperitoneal route
PLL Poly-L-lysine
PrP^C Normal, cellular isoform of the prion protein
PrP^{Sc} Infectious, disease-associated, pathogenic form of the prion protein
p-Stat3 Phosphorylated Signal Transducer and Activator of Transcription 3
Stat3 Signal Transducer and Activator of Transcription 3
SYP Synaptophysin
TAM 4-hydroxytamoxifen

Supplementary Information

The online version contains supplementary material available at <https://doi.org/10.1186/s40478-025-02028-6>.

Supplementary Material 1

Supplementary Material 2

Acknowledgements

We are grateful to Michael Sofroniew for his generous gift of Aldh111-CreERT-Stat3-floxP mouse model.

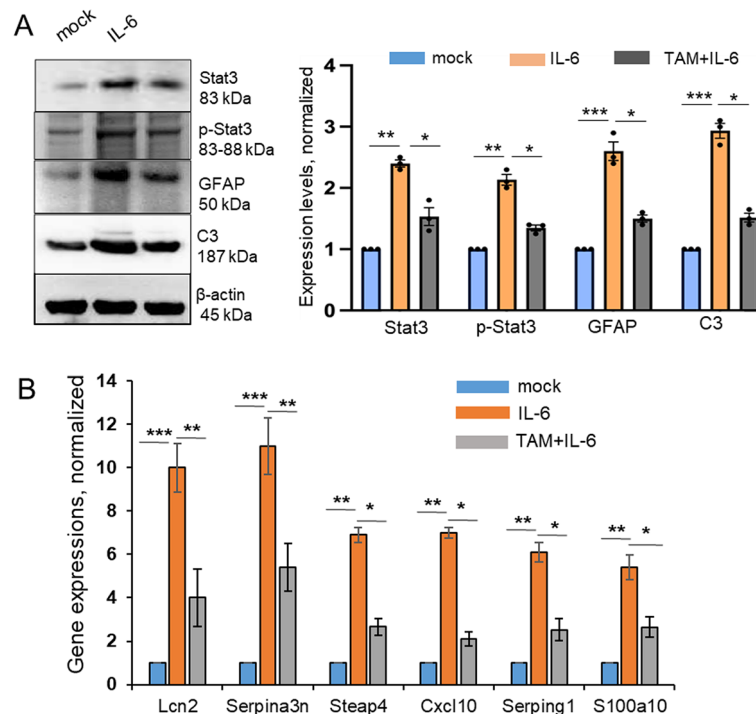


Fig. 7 IL-6 induces astrocyte reactivity in a Stat3-dependent manner. Astrocytes were isolated from non-infected, adult Cre^{+/-} mice, treated with IL-6, IL-6 and TAM or mock solution for 72 h and analyzed. **(A)** Representative Western blots and densitometric analysis of Stat3, p-Stat3, GFAP, and C3 expression normalized per expression of β-actin. **(B)** Analysis of expression of genes associated with astrocyte reactivity. Expression levels were normalized relative to the expression of the respective gene in mock-treated astrocytes. Data represent mean ± SE, ****p* < 0.001, ***p* < 0.01, **p* < 0.05, by one-way ANOVA with Bonferroni multiple comparisons post-hoc test, *N* = 3 independent astrocyte cultures per group, each originating from an individual animal

Author contributions

RK and IB designed the study; RK performed experiments; KM performed animal procedures and scored the disease signs; NM prepared 22 L brain homogenates; RK analyzed the data; IB and RK wrote the manuscript. All authors read, edited and approved the final manuscript.

Funding

Financial support for this study was provided by National Institute of Health Grants R01 NS045585 and R01 NS129502 to IVB.

Data availability

No datasets were generated or analysed during the current study.

Declarations**Ethics approval and consent to participate**

The study was carried out in strict accordance with the recommendations in the Guide for the Care and Use of Laboratory Animals of the National Institutes of Health. The animal protocol was approved by the Institutional Animal Care and Use Committee of the University of Maryland, Baltimore (Assurance Number: A32000-01; Protocol Numbers: 1120001 and 00000166-1).

Consent for publication

Not applicable.

Competing interests

The authors declare no competing interests.

Received: 28 January 2025 / Accepted: 1 May 2025

Published online: 15 May 2025

References

- Phatnani H, Maniatis T (2015) Astrocytes in neurodegenerative disease. *Cold Spring Harb Perspect Biol* 7(6)
- Ferrer I (2017) Diversity of astroglial responses across human neurodegenerative disorders and brain aging. *Brain Pathol* 27(5):645–674
- Habib N, McCabe C, Medina S, Varshavsky M, Kitsberg D, Dvir-Szternfeld R, Green G, Dionne D, Nguyen L, Marshall JL et al (2020) Disease-associated astrocytes in Alzheimer's disease and aging. *Nat Neurosci* 23(6):701–706
- Ben Haim L, Carrillo-de Sauvage M-A, Ceyzériat K, Escartin C (2015) Elusive roles for reactive astrocytes in neurodegenerative diseases. *Front Cell Neurosci* 9(278)
- Acioğlu C, Li L, Elkabes S (2021) Contribution of astrocytes to neuropathology of neurodegenerative diseases. *Brain Res*:147291
- Makarava N, Kushwaha R, Baskakov IV (2024) Reactive astrocytes in prion diseases: friend or foe? *PLoS Pathog* 20(6):e1012286
- Escartin C, Galea E, Lakatos A, O'Callaghan JP, Peltzold GC, Serrano-Pozo A, Steinhäuser C, Volterra A, Carmignoto G, Agarwal A et al (2021) Reactive astrocyte nomenclature, definitions, and future directions. *Nat Neurosci* 24(3):312–325
- Baskakov IV (2021) On the reactive States of astrocytes in prion diseases. *Prion* 15(1):87–93
- Sofroniew MV (2020) Astrocyte reactivity: subtypes, States, and functions in CNS innate immunity. *Trends Immunol* 41(9):758–770
- Prusiner SB (1998) Prions. *Proc Natl Acad Sci U S A* 95:13363–13383
- Giles K, Olson SH, Prusiner SB (2017) Developing therapeutics for PrP prion diseases. *Cold Spring Harb Perspect Med* 7(4)
- Prusiner SB (1982) Novel proteinaceous infectious particles cause scrapie. *Science* 216(4542):136–144
- Legname G, Baskakov IV, Nguyen HOB, Riesner D, Cohen FE, DeArmond SJ, Prusiner SB (2004) Synthetic mammalian prions. *Science* 305(5684):673–676
- Makarava N, Kovacs GG, Bocharova OV, Savtchenko R, Alexeeva I, Budka H, Rohrer RG, Baskakov IV (2010) Recombinant prion protein induces a new transmissible prion disease in wild type animals. *Acta Neuropathol* 119(2):177–187
- Wang F, Wang X, Yuan CG, Ma J (2010) Generating a prion bacterially expressed Recombinant prion protein. *Science* 327(5969):1132–1135
- Deleault NR, Harris BT, Rees JR, Supattapone S (2007) Formation of native prions from minimal components in vitro. *Proc Acad Natl Sci USA* 104(23):9741–9746
- Cohen FE, Prusiner SB (1998) Pathologic conformations of prion proteins. *Annu Rev Biochem* 67:793–819
- Makarava N, Chang JC-Y, Kushwaha R, Baskakov IV (2019) Region-Specific response of astrocytes to prion infection. *Front Neurosci* 13(1):e1048
- Makarava N, Mychko O, Chang JC-Y, Molesworth K, Baskakov IV (2021) The degree of astrocyte activation is predictive of the incubation time to prion disease. *Acta Neuropathol Commun* 9(1):87
- Makarava N, Chang JC-Y, Molesworth K, Baskakov IV (2020) Region-specific glial homeostatic signature in prion diseases is replaced by a uniform neuroinflammation signature, common for brain regions and prion strains with different cell tropism. *Neurobiol Dis* 137(1):e104783
- Scheckel C, Imeri M, Schwarz P, Aguzzi A (2020) Ribosomal profiling during prion disease uncovers progressive translational derangement in glia but not in neurons. *Elife* 9
- Kaczmarczyk L, Schleif M, Dittrich L, Williams RH, Koderman M, Bansal V, Rajput A, Schulte T, Jonson M, Krost C et al (2022) Distinct transcriptome changes in specific neural populations precede electroencephalographic changes in prion-infected mice. *PLoS Pathog* 18(8):e1010747
- Slota JA, Sajesh BV, Frost KF, Medina SJ, Booth SA (2022) Dysregulation of neuroprotective astrocytes, a spectrum of microglial activation States, and altered hippocampal neurogenesis are revealed by single-cell RNA sequencing in prion disease. *Acta Neuropathol Commun* 10(1):161
- Kushwaha R, Sinha A, Makarava N, Molesworth K, Baskakov IV (2021) Non-cell autonomous astrocyte-mediated neuronal toxicity in prion diseases. *Acta Neuropathol Commun* 9(1):22
- Kushwaha R, Li Y, Makarava N, Pandit NP, Molesworth K, Birukov KG, Baskakov IV (2023) Reactive astrocytes associated with prion disease impair the blood brain barrier. *Neurobiol Dis* 185:106264
- Smith HL, Freeman OJ, Butcher AJ, Holmqvist S, Humoud I, Schätzl T, Hughes DT, Verity NC, Swinden DP, Hayes J et al (2020) Astrocyte unfolded protein response induces a specific reactivity state that causes Non-Cell-Autonomous neuronal degeneration. *Neuron* 105(5):855–866e855
- Ben Haim L, Ceyzériat K, Carrillo-de Sauvage MA, Aubry F, Auregan G, Guillermier M, Ruiz M, Petit F, Houitte D, Faivre E et al (2015) The JAK/STAT3 pathway is a common inducer of astrocyte reactivity in Alzheimer's and Huntington's diseases. *J Neurosci* 35(6):2817–2829
- Ceyzériat K, Ben Haim L, Denizot A, Pommier D, Matos M, Guillemaud O, Palomares MA, Abjean L, Petit F, Gipchtein P et al (2018) Modulation of astrocyte reactivity improves functional deficits in mouse models of Alzheimer's disease. *Acta Neuropathol Commun* 6(1):104
- Reichenbach N, Delekate A, Plescher M, Schmitt F, Krauss S, Blank N, Halle A, Peltzold GC (2019) Inhibition of Stat3-mediated astrogliosis ameliorates pathology in an Alzheimer's disease model. *EMBO Mol Med* 11(2)
- Na Y-J, Jin J-K, Kim J-I, Choi E-K, Carp RI, Kim Y-S (2007) JAK-STAT signaling pathway mediates astrogliosis in brains of scrapie-infected mice. *J Neurochem* 103(2):637–649
- O'Shea TM, Ao Y, Wang S, Ren Y, Cheng AL, Kawaguchi R, Shi Z, Swarup V, Sofroniew MV (2024) Derivation and transcriptional reprogramming of border-forming wound repair astrocytes after spinal cord injury or stroke in mice. *Nat Neurosci* 27(8):1505–1521
- Makarava N, Safadi T, Bocharova O, Mychko O, Pandit NP, Molesworth K, Baiardi S, Zhang L, Parchi P, Baskakov IV (2024) Reactive microglia partially envelop viable neurons in prion diseases. *J Clin Invest* 134(23)
- Holt LM, Stoyanof ST, Olsen ML (2019) Magnetic cell sorting for in vivo and in vitro astrocyte, neuron, and microglia analysis. *Curr Protoc Neurosci* 88(1):e71
- Nikodemova M, Watters JJ (2012) Efficient isolation of live microglia with preserved phenotypes from adult mouse brain. *J Neuroinflammation* 9:147
- Leites EP, Morais VA (2024) Protocol for the isolation and culture of microglia, astrocytes, and neurons from the same mouse brain. *STAR Protoc* 5(1):102804
- Welsch JV, Milner R (2012) Use of astrocyte-microglial cocultures to examine the regulatory influence of astrocytes on microglial activation. *Methods Mol Biol* 814:367–380
- Viviani B, Corsini E, Galli CL, Marinovich M (1998) Glia increase degeneration of hippocampal neurons through release of tumor necrosis factor-alpha. *Toxicol Appl Pharmacol* 150(2):271–276
- Ippolito DM, Eroglu C (2010) Quantifying synapses: an immunocytochemistry-based assay to quantify synapse number. *J Vis Exp* 16(45):2270

39. Makarava N, Chang JC-Y, Molesworth K, Baskakov IV (2020) Posttranslational modifications define course of prion strain adaptation and disease phenotype. *J Clin Invest* 130(8):4382–4395
40. Hartmann K, Sepulveda-Falla D, Rose IVL, Madore C, Muth C, Matschke J, Butovsky O, Liddelov S, Glatzel M, Krasemann S (2019) Complement 3+ astrocytes are highly abundant in prion diseases, but their abolishment led to an accelerated disease course and early dysregulation of microglia. *Acta Neuropathol Commun* 7(1):83
41. Sorce S, Nuvoilone M, Russo G, Chincisan A, Heinzer D, Avar M, Pfammatter M, Schwarz P, Delic M, Müller M et al (2020) Genome-wide transcriptomics identifies an early preclinical signature of prion infection. *PLoS Pathog* 16(6):e1008653
42. Ashutosh, Chao C, Borgmann K, Brew K, Ghorpade A (2012) Tissue inhibitor of metalloproteinases-1 protects human neurons from staurosporine and HIV-1-induced apoptosis: mechanisms and relevance to HIV-1-associated dementia. *Cell Death Dis* 3(6):e332
43. Saha P, Sarkar S, Paidi RK, Biswas SC (2020) TIMP-1: A key cytokine released from activated astrocytes protects neurons and ameliorates cognitive behaviours in a rodent model of Alzheimer's disease. *Brain Behav Immun* 87:804–819
44. Huang B, Lang X, Li X (2022) The role of IL-6/JAK2/STAT3 signaling pathway in cancers. *Front Oncol* 12:1023177
45. Lashgari N-A, Roudsari NM, Momtaz S, Sathyapalan T, Abdolghaffari AH, Sahebkar A (2021) The involvement of JAK/STAT signaling pathway in the treatment of Parkinson's disease. *J Neuroimmunol* 361:577758
46. Lee JY, Park CS, Seo KJ, Kim IY, Han S, Youn I, Yune TY (2023) IL-6/JAK2/STAT3 axis mediates neuropathic pain by regulating astrocyte and microglia activation after spinal cord injury. *Exp Neurol* 370:114576
47. Dallérac G, Zapata J, Rouach N (2018) Versatile control of synaptic circuits by astrocytes: where, when and how? *Nat Rev Neurosci* 19(12):729–743
48. Santello M, Toni N, Volterra A (2019) Astrocyte function from information processing to cognition and cognitive impairment. *Nat Neurosci* 22(2):154–166
49. Sofroniew MV, Vinters HV (2010) Astrocytes: biology and pathology. *Acta Neuropathol* 119(1):7–35
50. Zeisel A, Hochgerner H, Lönnerberg P, Johnsson A, Memic F, van der Zwan J, Hargraves M, Braun E, Borm LE, La Manno G et al (2018) Molecular architecture of the mouse nervous system. *Cell* 174(4):999–1014
51. Ugalde CL, Lewis V, Stehmann C, McLean CA, Lawson VA, Collins SJ, Hill AF (2020) Markers of A1 astrocytes stratify to molecular sub-types in sporadic Creutzfeldt-Jakob disease brain. *Brain Commun* 2(2):fcaa029
52. Bradford BM, McGuire LI, Hume DA, Pridans C, Mabbott NA (2022) Microglia deficiency accelerates prion disease but does not enhance prion accumulation in the brain. *Glia* 70(11):2169–2187
53. Cameron EG, Nahmou M, Toth AB, Heo L, Tanasa B, Dalal R, Yan W, Nallagatla P, Xia X, Hay S et al (2023) A molecular switch for neuroprotective astrocyte reactivity. *Nature*
54. Liddelov SA, Guttenplan KA, Clarke LE, Bennett FC, Bohlen CJ, Schirmer L, Bennett ML, Munch AE, Chung WS, Peterson TC et al (2017) Neurotoxic reactive astrocytes are induced by activated microglia. *Nature* 541:481–487
55. Lian H, Yang L, Cole A, Sun L, Chiang AC, Fowler SW, Shim DJ, Rodriguez-Rivera J, Tagliatalata G, Jankowsky JL et al (2015) NF κ B-activated astroglial release of complement C3 compromises neuronal morphology and function associated with Alzheimer's disease. *Neuron* 85(1):101–115
56. Chi X, Yin S, Sun Y, Kou L, Zou W, Wang Y, Jin Z, Wang T, Xia Y (2025) Astrocyte-neuron communication through the complement C3-C3aR pathway in Parkinson's disease. *Brain Behav Immun* 123:229–243
57. Sun D, Qu J, Jakobs TC (2013) Reversible reactivity by optic nerve astrocytes. *Glia* 61(8):1218–1235
58. Hara M, Kobayakawa K, Ohkawa Y, Kumamaru H, Yokota K, Saito T, Kijima K, Yoshizaki S, Harimaya K, Nakashima Y et al (2017) Interaction of reactive astrocytes with type I collagen induces astrocytic Scar formation through the integrin-N-cadherin pathway after spinal cord injury. *Nat Med* 23(7):818–828
59. Pons-Espinal M, Blasco-Agell L, Fernandez-Carasa I, Andrés-Benito P, di Domenico A, Richaud-Patin Y, Baruffi V, Marruecos L, Espinosa L, Garrido A et al (2024) Blocking IL-6 signaling prevents astrocyte-induced neurodegeneration in an iPSC-based model of Parkinson's disease. *JCI Insight* 9(3)
60. Abjean L, Ben Haim L, Riquelme-Perez M, Gipchtein P, Derbois C, Palomares MA, Petit F, Hérard AS, Gaillard MC, Guillemier M et al (2023) Reactive astrocytes promote proteostasis in Huntington's disease through the JAK2-STAT3 pathway. *Brain* 146(1):149–166
61. Linnerbauer M, Wheeler MA, Quintana FJ (2020) Astrocyte crosstalk in CNS inflammation. *Neuron* 108(4):608–622
62. Matejuk A, Ransohoff RM (2020) Crosstalk between astrocytes and microglia: an overview. *Front Immunol* 11:1416
63. Carroll JA, Race B, Williams K, Striabel J, Chesebro B (2018) Microglia are critical in host defense against prion disease. *J Virol* 92(15):e00549–e00518
64. Carroll JA, Race B, Williams K, Striabel J, Chesebro B (2020) RNA-seq and network analysis reveal unique glial gene expression signatures during prion infection. *Mol Brain* 13(1):71
65. Zhu C, Herrmann US, Falsig J, Abakumova I, Nuvoilone M, Schwarz P, Frauenknecht K, Rushing EJ, Aguzzi A (2016) A neuroprotective role for microglia in prion diseases. *J Exp Med* 213(6):1047–1059
66. Jung YJ, Tweedie D, Scerba MT, Greig NH (2019) Neuroinflammation as a factor of neurodegenerative disease: thalidomide analogs as treatments. *Front Cell Dev Biol* 7:313
67. Guzman-Martinez L, Maccioni RB, Andrade V, Navarrete LP, Pastor MG, Ramos-Escobar N (2019) Neuroinflammation as a common feature of neurodegenerative disorders. *Front Pharmacol* 10:1008
68. Sarkar S, Gharami K, Paidi RK, Sri Kumar BN, Biswas SC An astrocyte-derived cytokine TIMP-1 restores synaptic plasticity in an Alzheimer's disease model. *bioRxiv* 2023:2023.2003.2018.533245.
69. Andreadou M, Ingelfinger F, De Feo D, Cramer TLM, Tuzlak S, Friebe E, Schreiner B, Eede P, Schneeberger S, Geesdorf M et al (2023) IL-12 sensing in neurons induces neuroprotective CNS tissue adaptation and attenuates neuroinflammation in mice. *Nat Neurosci* 26(10):1701–1712
70. Vom Berg J, Prokop S, Miller KR, Obst J, Kälin RE, Lopategui-Cabezas I, Wegner A, Mair F, Schipke CG, Peters O et al (2012) Inhibition of IL-12/IL-23 signaling reduces Alzheimer's disease-like pathology and cognitive decline. *Nat Med* 18(12):1812–1819
71. Kummer KK, Zeidler M, Kalpachidou T, Kress M (2021) Role of IL-6 in the regulation of neuronal development, survival and function. *Cytokine* 144:155582
72. Chucair-Elliott AJ, Conrady C, Zheng M, Kroll CM, Lane TE, Carr DJ (2014) Microglia-induced IL-6 protects against neuronal loss following HSV-1 infection of neural progenitor cells. *Glia* 62(9):1418–1434
73. Lyra e Silva NM, Gonçalves RA, Pascoal TA, Lima-Filho RAS, Resende EPF, Vieira ELM, Teixeira AL, de Souza LC, Peny JA, Fortuna JTS et al (2021) Pro-inflammatory interleukin-6 signaling links cognitive impairments and peripheral metabolic alterations in Alzheimer's disease. *Translational Psychiatry* 11(1):251
74. Diaz K, Kohut ML, Russell DW, Stegemöller EL (2022) Peripheral inflammatory cytokines and motor symptoms in persons with Parkinson's disease. *Brain, Behavior, & Immunity - Health* 21:100442
75. Bauer J, Strauss S, Schreiter-Gasser U, Ganter U, Schlegel P, Witt I, Yolk B, Berger M (1991) Interleukin-6 and alpha-2-macroglobulin indicate an acute-phase state in Alzheimer's disease cortices. *FEBS Lett* 285(1):111–114
76. Mogi M, Harada M, Kondo T, Riederer P, Inagaki H, Minami M, Nagatsu T (1994) Interleukin-1 β , interleukin-6, epidermal growth factor and transforming growth factor- α are elevated in the brain from parkinsonian patients. *Neurosci Lett* 180(2):147–150
77. Maimone D, Guazzi GC, Annunziata P (1997) IL-6 detection in multiple sclerosis brain. *J Neurol Sci* 146(1):59–65
78. Rothaug M, Becker-Pauly C, Rose-John S (2016) The role of interleukin-6 signaling in nervous tissue. *Biochim Et Biophys Acta (BBA) - Mol Cell Res* 1863(6):1218–1227 Part A)
79. Campbell IL, Erta M, Lim SL, Frausto R, May U, Rose-John S, Scheller J, Hidalgo J (2014) Trans-signaling is a dominant mechanism for the pathogenic actions of interleukin-6 in the brain. *J Neurosci* 34(7):2503–2513
80. Campbell IL, Abraham CR, Masliah E, Kemper P, Inglis JD, Oldstone MB, Mucke L (1993) Neurologic disease induced in Transgenic mice by cerebral overexpression of Interleukin 6. *Proc Natl Acad Sci U S A* 90(21):10061–10065
81. Srivastava S, Katorcha E, Makarava N, Barrett JP, Loane DJ, Baskakov IV (2018) Inflammatory response of microglia to prions is controlled by sialylation of PrP^{Sc}. *Sci Rep* 8(1):e11326
82. Burda JE, O'Shea TM, Ao Y, Suresh KB, Wang S, Bernstein AM, Chandra A, Deverasetty S, Kawaguchi R, Kim JH et al (2022) Divergent transcriptional regulation of astrocyte reactivity across disorders. *Nature* 606(7914):557–564
83. Makarava N, Mychko O, Molesworth K, Chang JC, Henry RJ, Tsybalyuk N, Gerzanich V, Simard JM, Loane DJ, Baskakov IV (2023) Region-Specific homeostatic identity of astrocytes is essential for defining their response to pathological insults. *Cells* 12(17)
84. Hidano S, Randall Louise M, Dawson L, Dietrich Hans K, Konradt C, Klover Peter J, John B, Harris Tajie H, Fang Q, Turek B et al (2016) STAT1 signaling in astrocytes is essential for control of infection in the central nervous system. *mBio* 7(6). <https://doi.org/10.1128/mbio.01881-01816>

85. Khorroshi R, Babcock AA, Owens T (2008) NF-kappaB-driven STAT2 and CCL2 expression in astrocytes in response to brain injury. *J Immunol* 181(10):7284–7291

Publisher's note

Springer Nature remains neutral with regard to jurisdictional claims in published maps and institutional affiliations.